© 2018. Published by The Company of Biologists Ltd | Development (2018) 145, dev159210. doi:10.1242/dev.159210

RESEARCH ARTICLE

The Hippo pathway effector Wwtr1 regulates cardiac wall maturation in zebrafish

Jason K. H. Lai[1], Michelle M. Collins[1], Veronica Uribe[1], Vanesa Jiménez-Amilburu[1], Stefan Günther[2], Hans-Martin Maischein[1] and Didier Y. R. Stainier[1,*]

ABSTRACT

Cardiac trabeculation is a highly regulated process that starts with the delamination of compact layer cardiomyocytes. The Hippo signaling pathway has been implicated in cardiac development but many questions remain. We have investigated the role of Wwtr1, a nuclear effector of the Hippo pathway, in zebrafish and find that its loss leads to reduced cardiac trabeculation. However, in mosaic animals, *wwtr1*$^{-/-}$ cardiomyocytes contribute more frequently than *wwtr1*$^{+/-}$ cardiomyocytes to the trabecular layer of wild-type hearts. To investigate this paradox, we examined the myocardial wall at early stages and found that compact layer cardiomyocytes in *wwtr1*$^{-/-}$ hearts exhibit disorganized cortical actin structure and abnormal cell-cell junctions. Accordingly, wild-type cardiomyocytes in mosaic mutant hearts contribute less frequently to the trabecular layer than when present in mosaic wild-type hearts, indicating that *wwtr1*$^{-/-}$ hearts are not able to support trabeculation. We also found that Nrg/Erbb2 signaling, which is required for trabeculation, could promote Wwtr1 nuclear export in cardiomyocytes. Altogether, these data suggest that Wwtr1 establishes the compact wall architecture necessary for trabeculation, and that Nrg/Erbb2 signaling negatively regulates its nuclear localization and therefore its activity.

KEY WORDS: Heart development, Hippo pathway, Yap, Taz, Wwtr1, Trabeculation

INTRODUCTION

Cardiac trabeculation is an important step to cardiac wall maturation and is key to the growth and function of the heart (Ozcelik et al., 2002; García-Rivello et al., 2005; Liu et al., 2010; Staudt and Stainier, 2012). During cardiac development, both the endocardial and myocardial layers participate in a series of signaling pathways that lead to the formation of a trabeculated ventricle. Cardiac trabeculation requires the neuregulin signaling pathway, as mutants (mouse, *Nrg1* and *Erbb2/4*; zebrafish, *nrg2a* and *erbb2*) affected in this pathway lack trabecular structures (Gassmann et al., 1995; Lee et al., 1995; Meyer and Birchmeier, 1995; Liu et al., 2010; Rasouli and Stainier, 2017). Neuregulin ligands, which are expressed by endocardial cells (Meyer and Birchmeier, 1995; Grego-Bessa et al., 2007; Rasouli and Stainier, 2017), stimulate cardiomyocytes through ERBB2/4 receptors (Gassmann et al., 1995; Lee et al., 1995; Liu et al., 2010) to delaminate from the compact layer (Staudt et al., 2014). Nrg/Erbb2 signaling also drives cardiomyocyte proliferation (Bersell et al., 2009; Xin et al., 2013a; D'Uva et al., 2015). In mouse, the expression of neuregulin is modulated by Notch activity, as conditional deletion of Notch1, or its co-factor RBPJk, in the endothelium results in downregulation of *Nrg1* expression (Grego-Bessa et al., 2007). In zebrafish, mutants/morphants with defective cardiac contractility exhibit hearts with reduced *nrg2a* expression (Rasouli and Stainier, 2017), which explains why *tnnt2a* (*silent heart*/*sih*) mutant hearts lack trabeculae (Chi et al., 2008; Samsa et al., 2015). However, many questions remain regarding how neuregulin signaling affects cardiomyocyte behavior during delamination and cardiac trabeculation.

YAP1 and WWTR1 (also known as TAZ) are nuclear effectors of the Hippo signaling pathway, and their nuclear localization and association with TEADs promote cell proliferation and survival (Johnson and Halder, 2014; Yu et al., 2015). The Hippo kinase cassette is a negative regulator of YAP1/WWTR1 activity (Wu et al., 2003; Huang et al., 2005; Zhao et al., 2010), and constitutive activity of YAP1/WWTR1 can lead to uncontrolled growth and/or tumorigenesis (Lu et al., 2010; Cox et al., 2016). The Hippo signaling pathway has been a topic of intense investigation in recent years, unveiling new discoveries for YAP1/WWTR1 function, such as modulating cell behavior (Kim et al., 2017; Kimelman et al., 2017) and metabolism (Cox et al., 2016; Kim et al., 2017), during development. The Hippo signaling pathway is also known to interact with other signaling pathways that participate in cardiac trabeculation. For example, YAP1 has been reported to interact with the intracellular domain of ERBB4, and the complex is shuttled into the nucleus by neuregulin stimulation (Komuro et al., 2003; Haskins et al., 2014). YAP1 also interacts with the Notch intracellular domain (NICD) (Manderfield et al., 2015), and recent studies have further shown that YAP1/WWTR1 can drive the expression of Notch ligands (Totaro et al., 2017), including *JAG2* in chick skeletal muscle (Esteves de Lima et al., 2016). Additionally, the nuclear localization of YAP1 is regulated by mechanical forces, including skeletal muscle contraction (Esteves de Lima et al., 2016) and blood flow (Nakajima et al., 2017). However, previous studies investigating the Hippo signaling pathway and YAP1 in heart development have mostly focused on myocardial growth (Heallen et al., 2011; Xin et al., 2011; von Gise et al., 2012) and regeneration (Xin et al., 2013b; Heallen et al., 2013). Furthermore, the function of WWTR1, a vertebrate paralog of YAP1 (Hilman and Gat, 2011), in heart development has not been studied, leaving many questions about the Hippo signaling pathway during heart development unanswered. Thus, we used the zebrafish model in this study to investigate the role of Wwtr1 in cardiac development.

In the developing zebrafish heart, we find that Wwtr1 is predominantly localized to the nuclei of compact wall cardiomyocytes and, to a lesser extent to those of trabecular layer

[1]Max Planck Institute for Heart and Lung Research, Department of Developmental Genetics, Bad Nauheim 61231, Germany. [2]Max Planck Institute for Heart and Lung Research, ECCPS Bioinformatics and Deep Sequencing Platform, Bad Nauheim 61231, Germany.

*Author for correspondence (didier.stainier@mpi-bn.mpg.de)

D.Y.R.S., 0000-0002-0382-0026

Received 7 September 2017; Accepted 23 April 2018

Development (2018) 145, dev159210. doi:10.1242/dev.159210

cardiomyocytes. In agreement with these observations, *wwtr1*$^{-/-}$ cardiomyocytes in mosaic wild-type hearts prefer to populate the trabecular layer. However, we also find that *wwtr1*$^{-/-}$ hearts exhibit reduced trabeculation. Investigating this paradox led to novel insights into the function of the Hippo signaling pathway, and specifically Wwtr1, during vertebrate heart development, especially in cardiac wall maturation.

RESULTS

Nuclear localization of Wwtr1 in ventricular compact wall cardiomyocytes

We first investigated the spatiotemporal expression pattern of Wwtr1 in the developing zebrafish heart by immunostaining. An antibody against human WWTR1 (which cross-reacts with human YAP1) has been shown, using zebrafish *wwtr1* mutant embryos as negative controls, to recognize zebrafish Wwtr1 in a number of tissues, including the periocular mesenchyme (Miesfeld et al., 2015), ectoderm and notochord (Kimelman et al., 2017) and, in this study, the heart (Fig. S1A). During embryonic and early larval stages, i.e. from 30 to 119 hours post fertilization (hpf), we observed that Wwtr1 immunostaining was predominantly localized to the nuclei of ventricular cardiomyocytes (Fig. 1). During the onset of trabeculation from 60 to 72 hpf, nuclei of delaminating or trabecular cardiomyocytes exhibited weaker Wwtr1 immunostaining than those of adjacent compact layer cardiomyocytes (cross-sections of Fig. 1B, and Fig. S1B).

Zebrafish *wwtr1* mutants do not form mature trabecular ridges

To study the function of Wwtr1 during zebrafish heart development, we generated a *wwtr1* mutant using the CRISPR/CAS9 technology and identified an allele with a 29 bp insertion in exon 2 (*wwtr1*^{bns35}). This out-of-frame insertion is predicted to cause the production of a truncated protein (p.Pro145Glnfs*15) (Fig. 2A). The mutant transcript was also less abundant than the wild-type transcript, as assessed by real-time PCR of whole embryos (data not shown) and RNA sequencing (RNAseq) of embryonic hearts (Table S1), suggesting nonsense-mediated decay. At 96 hpf, the luminal surface of *wwtr1*$^{-/-}$ hearts was mostly smooth, appearing to lack the trabecular structures that line the outer-curvature of the wild-type ventricle (Fig. 2B). These trabecular structures are observed as 'finger-like' multicellular protrusions in a mid-sagittal confocal plane of wild-type animals (Fig. 2C). In contrast, the *wwtr1*$^{-/-}$ ventricular wall, although composed of multiple layers of cardiomyocytes, did not exhibit 'finger-like' protrusions (Fig. 2C). To quantify ventricular cardiomyocytes, we first determined their total number and then separated them into two groups: the outermost layer cardiomyocytes (designated as compact wall cardiomyocytes); and the innermost layer cardiomyocytes (designated as trabecular layer cardiomyocytes). The number of cardiomyocytes in the trabecular layer of *wwtr1*$^{-/-}$ hearts was significantly reduced at all stages examined (Fig. 2D), probably as a result of reduced delamination as well as reduced proliferation in the trabecular layer, as assessed by EdU incorporation (Fig. S2).

We have previously shown that inhibiting the neuregulin signaling pathway results in fewer cardiomyocytes undergoing apical constriction at 82-100 hpf (Jiménez-Amilburu et al., 2016), consistent with the lack of trabeculae in *nrg2a/erbb2* mutant hearts. In contrast, we did not observe a significant change in the number of cardiomyocytes undergoing apical constriction in *wwtr1*$^{-/-}$ hearts at 79 hpf when compared with wild type (Fig. S3A,B). Once cardiomyocytes undergo apical constriction and enter the trabecular layer, they are usually depolarized, as assessed by the localization of an EGFP-Podxl transgene; some cardiomyocytes may repolarize, but will eventually depolarize again (Jiménez-Amilburu et al., 2016). Although the majority of trabecular cardiomyocytes in both *wwtr1*$^{-/-}$ and wild-type sibling hearts were depolarized, we found a twofold increase in the percentage of polarized cardiomyocytes in the trabecular layer of *wwtr1*$^{-/-}$ hearts (Fig. S3C,D). In order to mosaically label cardiomyocytes in 96 hpf *wwtr1* mutant and wild-type sibling hearts, we injected a *myl7:mKate* plasmid into one-cell stage embryos. We selected trabecular layer cardiomyocytes and visualized the expression pattern of *myl7:*LIFEACT-GFP. Cardiomyocytes in the trabecular layer of 96 hpf *wwtr1*$^{-/-}$ hearts appeared flat and did not form any appreciable striated sarcomeric actin (Fig. S3E), in contrast to trabecular cardiomyocytes in wild-type hearts. In summary, *wwtr1*$^{-/-}$ hearts exhibited reduced trabeculation and abnormal trabecular morphology.

Myocardial Notch activity is modulated by Wwtr1 in a cell-autonomous manner

Notch signaling has been associated with multiple steps of cardiac trabeculation (Grego-Bessa et al., 2007; Samsa et al., 2015; D'Amato et al., 2016; Han et al., 2016; Jiménez-Amilburu et al., 2016). Therefore, we investigated Notch signaling in *wwtr1*$^{-/-}$ hearts by using a Notch reporter that expresses destabilized Venus under the control of the Notch-responsive *tp1* element (Ninov et al., 2012). At 48 hpf, *tp1* Notch reporter expression was present throughout the ventricular endocardium of *wwtr1*$^{+/+}$ and *wwtr1*$^{-/-}$ hearts (data not shown) as reported before in wild-type hearts (Samsa et al., 2015). However, at 72 and 96 hpf, whereas a subset of compact layer cardiomyocytes in *wwtr1*$^{+/+}$ and *wwtr1*$^{+/-}$ hearts expressed the *tp1* Notch reporter, cardiomyocytes in most (7/8) *wwtr1*$^{-/-}$ hearts did not (Fig. 3A,B). A zebrafish *jag2b* mutant was similarly reported to lack expression of the *tp1* Notch reporter in cardiomyocytes (Han et al., 2016). In contrast to the reported hypertrabeculation phenotype (Han et al., 2016), we found that *jag2b* mutant hearts exhibited reduced trabeculation (Fig. S4), a phenotype similar to that of *wwtr1* mutant hearts. In addition, we found that the majority of *tp1*$^{+}$ cardiomyocytes exhibited nuclear localization of Wwtr1 (Fig. S5A), further suggesting that Wwtr1 plays a role in cardiomyocyte expression of the *tp1* Notch reporter. We performed cell transplantation experiments to investigate whether Wwtr1 drives cardiomyocyte expression of the *tp1* Notch reporter in a cell-autonomous manner. When wild-type cells were transplanted into *wwtr1*$^{+/-}$ or *wwtr1*$^{-/-}$ hosts, wild-type and *wwtr1*$^{+/-}$, but not *wwtr1*$^{-/-}$, cardiomyocytes could express the *tp1* Notch reporter (Fig. 3C,C′). Conversely, when *wwtr1*$^{+/-}$ or *wwtr1*$^{-/-}$ cells were transplanted into wild-type hosts, again both wild-type and *wwtr1*$^{+/-}$, but not *wwtr1*$^{-/-}$, cardiomyocytes could express the *tp1* Notch reporter (Fig. 3D,D′). These data indicate that Wwtr1 modulates cardiomyocyte expression of the *tp1* Notch reporter in a cell-autonomous manner. We then mosaically expressed in *wwtr1*$^{-/-}$ cardiomyocytes, wild-type Wwtr1, as well as Wwtr1 variants that affect the WW domain (WW*: W142A, P145A) (Linn et al., 1997) or Tead-binding domain (TBD*: S48A; ΔTBD: P46_D65del) (Vassilev et al., 2001; Zhao et al., 2008; Miesfeld et al., 2015) (Fig. S5B). Whereas some *wwtr1*$^{-/-}$ cardiomyocytes that expressed the WT or WW* constructs of Wwtr1 were *tp1*$^{+}$, *wwtr1*$^{-/-}$ cardiomyocytes that expressed the TBD* or ΔTBD constructs mostly remained *tp1*$^{-}$ (Fig. S5C,D), suggesting that the Tead-binding domain of Wwtr1 is required for *tp1* Notch reporter expression in cardiomyocytes.

Development (2018) 145, dev159210. doi:10.1242/dev.159210

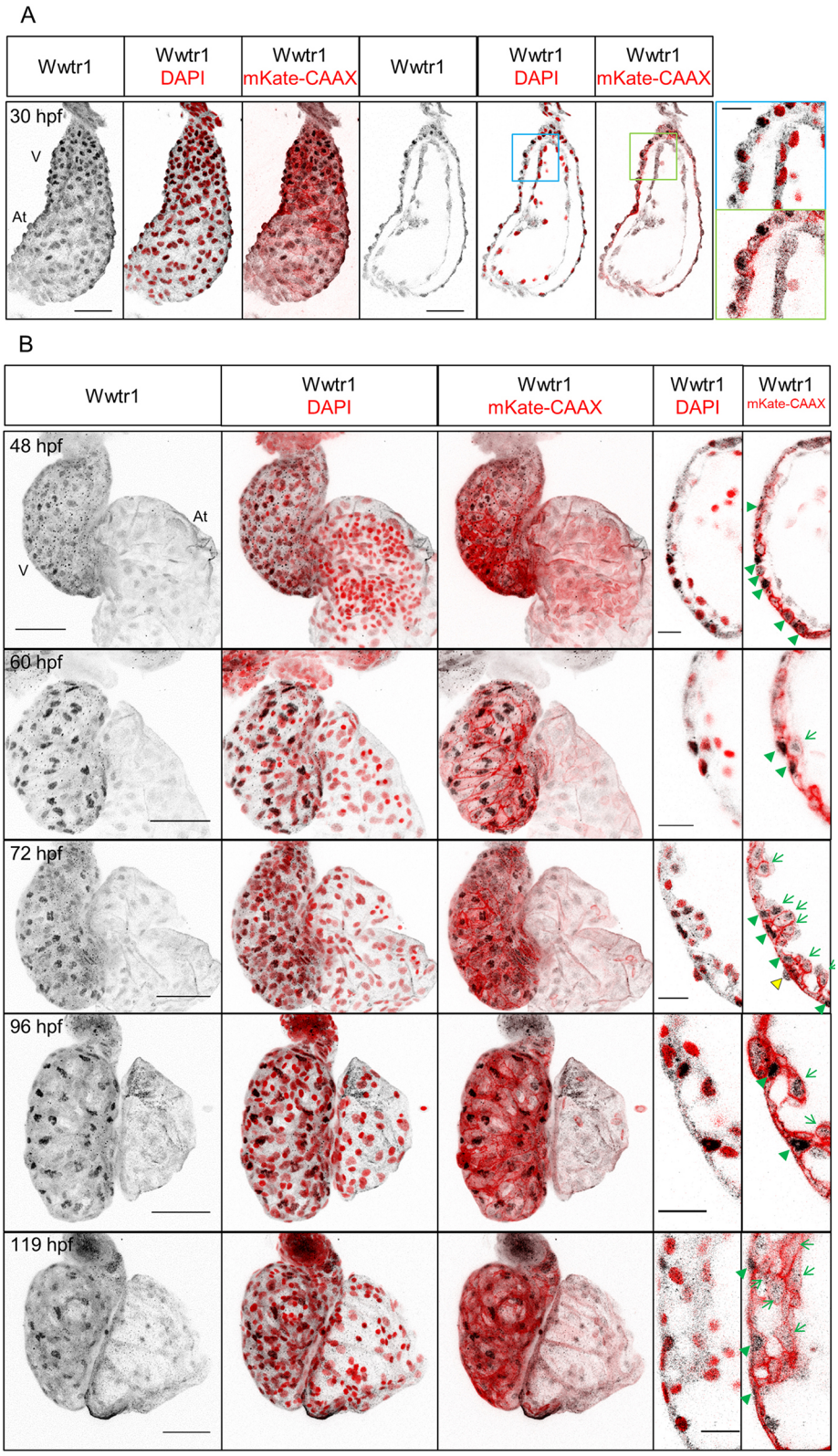

Fig. 1. Expression and localization of Wwtr1 in the developing zebrafish heart. (A) Maximum intensity projections and confocal sagittal sections of a whole-mount zebrafish heart at 30 hpf. Magnified images (blue and green squares) show that the nuclei of cardiomyocytes, but not of endocardial cells, are positive for Wwtr1 expression. (B) Maximum intensity projections and confocal sagittal sections of whole-mount zebrafish hearts from 48 to 119 hpf. Wwtr1 is predominantly localized in the nucleus in some ventricular cardiomyocytes (green arrowheads) and moderately expressed in some epicardial cells (yellow arrowhead), but absent from endocardial cells. During trabeculation, some cardiomyocytes delaminate from the compact layer and exhibit weaker nuclear staining for Wwtr1 compared with adjacent compact layer cardiomyocytes (green arrows and Fig. S1B). Nuclei are counterstained with DAPI and cardiomyocyte membranes are marked with *myl7:* mKate-CAAX expression. Scale bars: 50 µm; 15 µm (insets). V, ventricle; At, atrium. 30-72 hpf, n>3. 96 and 119 hpf, n=2.

Wwtr1 activity modulates cardiomyocyte egress from the compact layer

Surprisingly, in the above-mentioned transplant experiments, we observed that *wwtr1*$^{-/-}$ cardiomyocytes were able to contribute to the trabecular layer of wild-type hearts. In fact, we found that *wwtr1*$^{-/-}$ cardiomyocytes were located more frequently than *wwtr1*$^{+/-}$ cardiomyocytes in the trabecular layer of mosaic wild-type hearts (Fig. 4A, Fig. S6A). Conversely, wild-type cardiomyocytes were located less frequently in the trabecular layer of *wwtr1*$^{-/-}$ than *wwtr1*$^{+/-}$ hearts (Fig. 4B, Fig. S6B). As described earlier, Wwtr1 immunostaining appears weaker in the nuclei of trabecular cardiomyocytes than in those of compact layer

Development (2018) 145, dev159210. doi:10.1242/dev.159210

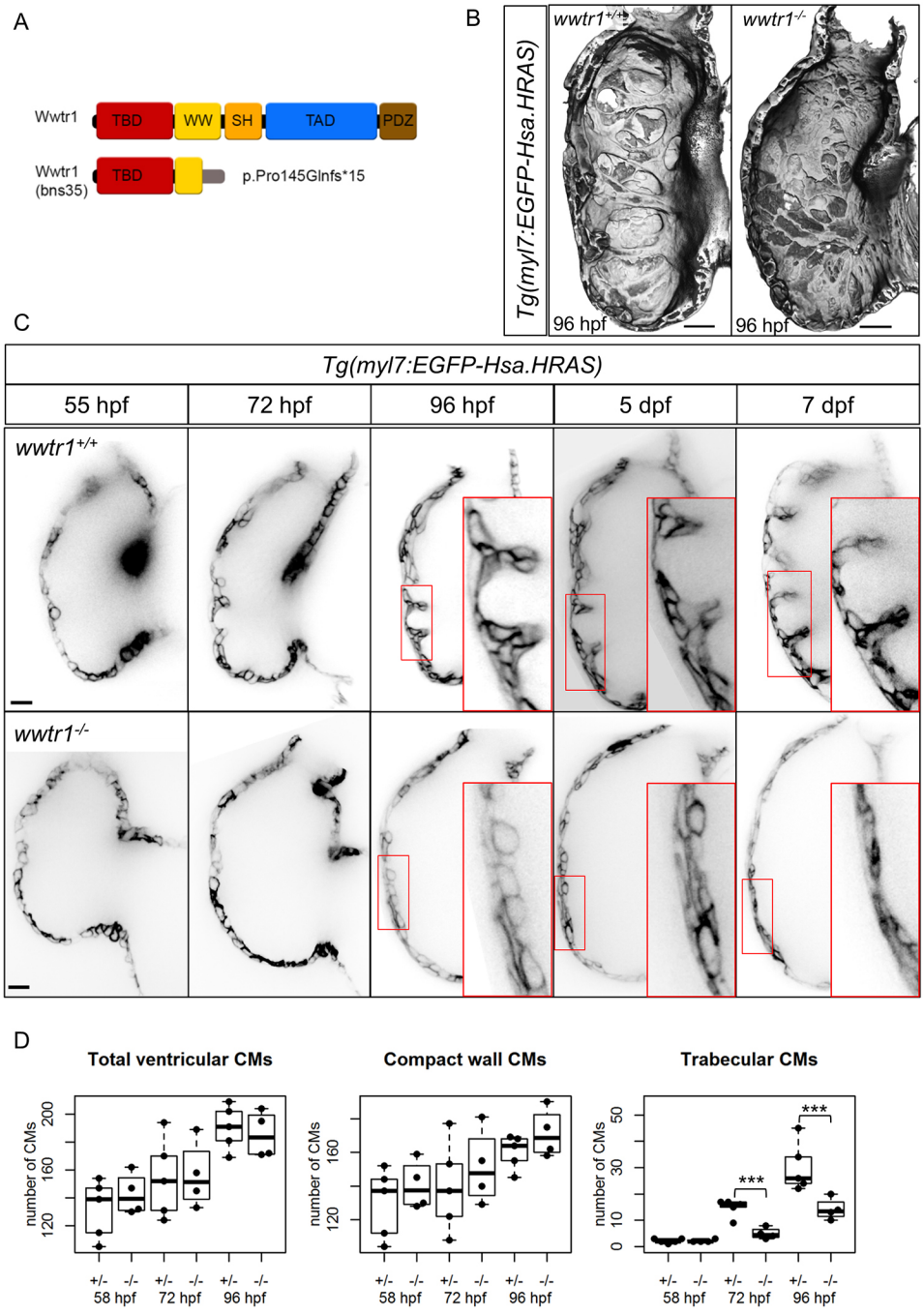

Fig. 2. *wwtr1* mutant hearts do not develop trabecular ridges. (A) Schematic of wild-type and predicted truncation of Wwtr1 due to a CRISPR-induced out-of-frame insertion (see Materials and Methods). (B) 3D surface reconstruction of ventricular chambers at 96 hpf shows distinct and prominent muscular ridges in *wwtr1*$^{+/+}$ (8/8) and *wwtr1*$^{+/-}$ (7/7), but not *wwtr1*$^{-/-}$ (20/24), hearts. Scale bars: 15 µm. (C) Confocal sagittal sections of wild-type and *wwtr1*$^{-/-}$ ventricular chambers of the same animal from 55 hpf to 7 dpf. Scale bars: 15 µm. (D) Longitudinal quantification of the number of ventricular cardiomyocytes (CMs) from five *wwtr1*$^{+/-}$ and four *wwtr1*$^{-/-}$ hearts. The total number of ventricular CMs is divided into two groups: compact wall CMs and trabecular CMs. Each point represents a heart. ***P<0.001 by Poisson regression. The box covers the inter-quartile range (IQR); the whiskers cover the first and last quartile of the data. Data points outside the whiskers are outliers (>1.5×IQR from the first and third quartile).

cardiomyocytes (Fig. S1B), raising the possibility that Wwtr1 activity modulates the likelihood of a cardiomyocyte to leave the compact layer. We tested this model further using a gain-of-function approach with a constitutively active Wwtr1 (CAWwtr1) [Wwtr1 S79A, which is homologous to Yap1 S87A (Cox et al., 2016)] (Fig. 4C). The S79 residue of Wwtr1 is part of the HXRXXS motif, which, when phosphorylated by Lats1/2, leads to the nuclear export of Wwtr1 (Zhao et al., 2010). We mosaically expressed *myl7:*mKate (control) or *myl7:*mKate-2A-CAWwtr1 and found that cardiomyocytes expressing mKate-2A-CAWwtr1 ended up in the trabecular layer less frequently than control (Fig. 4C′,C″, Fig. S6C). Altogether, these data indicate that Wwtr1 can modulate the likelihood of a cardiomyocyte to egress the compact layer and seed the trabecular layer.

Wwtr1 is required in the myocardium for compact wall morphogenesis

Wild-type cardiomyocytes were observed less frequently in the trabecular layer of mosaic *wwtr1*$^{-/-}$ hearts, possibly indicating defects in the development of the compact wall in mutant hearts. Therefore, we investigated the cellular morphology and actomyosin network of cardiomyocytes prior to trabeculation. Compact wall cardiomyocytes in wild-type hearts are rich in basally localized cortical actin exhibiting striated patterns (Reischauer et al., 2014) (Fig. 5A,B). In contrast, compact wall cardiomyocytes in *wwtr1*$^{-/-}$ hearts did not exhibit regular striations across their cortical actin bundles (Fig. 5B), and these bundles appeared thinner than wild type (Fig. 5C). Moreover, phospho-MRLC (pMRLC) immunostaining intensity appeared weaker in *wwtr1*$^{-/-}$ than

Development (2018) 145, dev159210. doi:10.1242/dev.159210

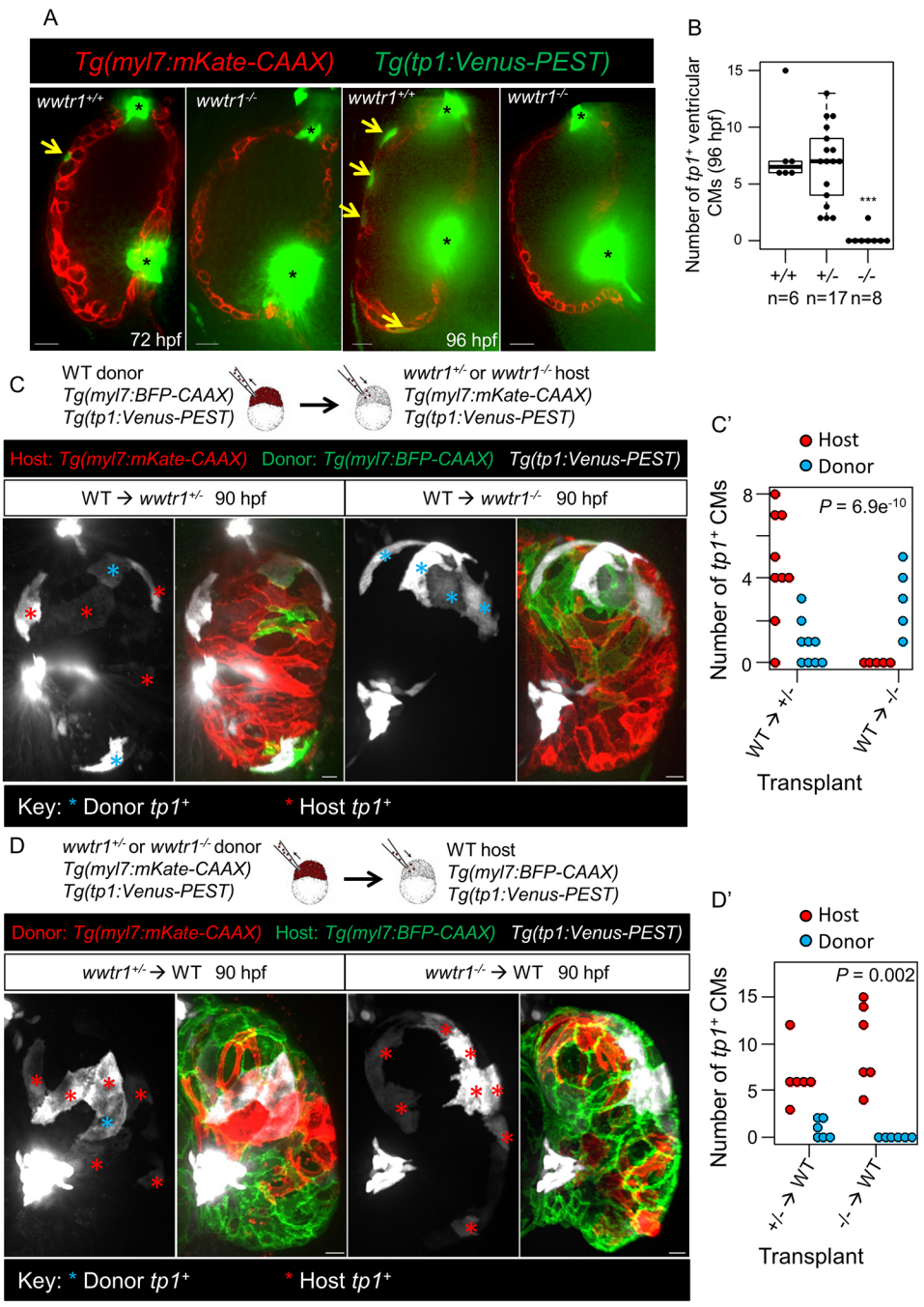

Fig. 3. Wwtr1 functions cell-autonomously in cardiomyocytes to regulate *tp1* Notch reporter expression. (A) Confocal sagittal sections of representative ventricular chambers at 72 and 96 hpf. Yellow arrows indicate cardiomyocytes expressing the *tp1* Notch reporter. The out of focus green signal is from endocardial cells at the valve regions (asterisks). Scale bars: 15 µm. (B) Number of $tp1^{+}$ ventricular cardiomyocytes at 96 hpf. Each point represents a heart. ***P<0.001 by Poisson regression. (C,D) Maximum intensity projections of hearts derived from transplanting wild-type cells into $wwtr1^{+/-}$ or $wwtr1^{-/-}$ hosts (C), and vice versa (D). Scale bars: 10 µm. (C′,D′) Number of $tp1^{+}$ donor and host cardiomyocytes (CMs) according to the respective transplantation schemes, as indicated on the *x*-axis. Each point represents a heart. *P*-values were calculated using an exact Binomial test. The box covers the inter-quartile range (IQR); the whiskers cover the first and last quartile of the data. Data points outside the whiskers are outliers (>1.5×IQR from the first and third quartile).

$wwtr1^{+/+}$ hearts (Fig. S7A). As these phenotypes could be secondary to defects in cardiac function, we examined the mutant hearts more closely, and although heart rate was reduced at 52 hpf, cardiac contraction was not obviously affected (Fig. S7B, Movie 1). We also examined actomyosin morphology shortly after Wwtr1 immunostaining in cardiomyocytes becomes evident (i.e. 30 hpf), and did not observe overt aberrations in mutant cardiomyocytes at this stage (Fig. S7C).

In 52 hpf wild-type hearts, N-cadherin-GFP is localized at the junctions between cardiomyocytes (Cherian et al., 2016); in $wwtr1^{-/-}$ hearts, it appeared to distribute in a punctate manner over the apical and basal surfaces of some cardiomyocytes (Fig. 5D). However, analysis of optical cross-sections of regions showing aberrant N-cadherin-GFP localization revealed that it was present at the junctions of $wwtr1^{-/-}$ cardiomyocytes, but that the lateral membranes were oblique to the apical surface and not perpendicular, as in wild type (Fig. 5E-G). Looking at earlier stages (30 hpf), N-cadherin-GFP localization did not appear to be affected in $wwtr1^{-/-}$ hearts (Fig. S7D). Apicobasal polarity of compact layer cardiomyocytes in $wwtr1^{-/-}$ hearts did not appear to be affected either, as assessed by EGFP-Podxl and Mark3a-tagRFPt transgene localization, at least at 52 hpf (Fig. S8). Altogether, these data indicate that Wwtr1 plays a role in compact wall morphogenesis prior to the emergence of trabeculae, specifically in the way cardiomyocytes organize their cortical actin networks and orient their lateral membranes in relation to the apicobasal axis.

To identify genes differentially regulated in $wwtr1^{-/-}$ hearts, we compared their transcriptome with that of wild-type sibling hearts at

Development (2018) 145, dev159210. doi:10.1242/dev.159210

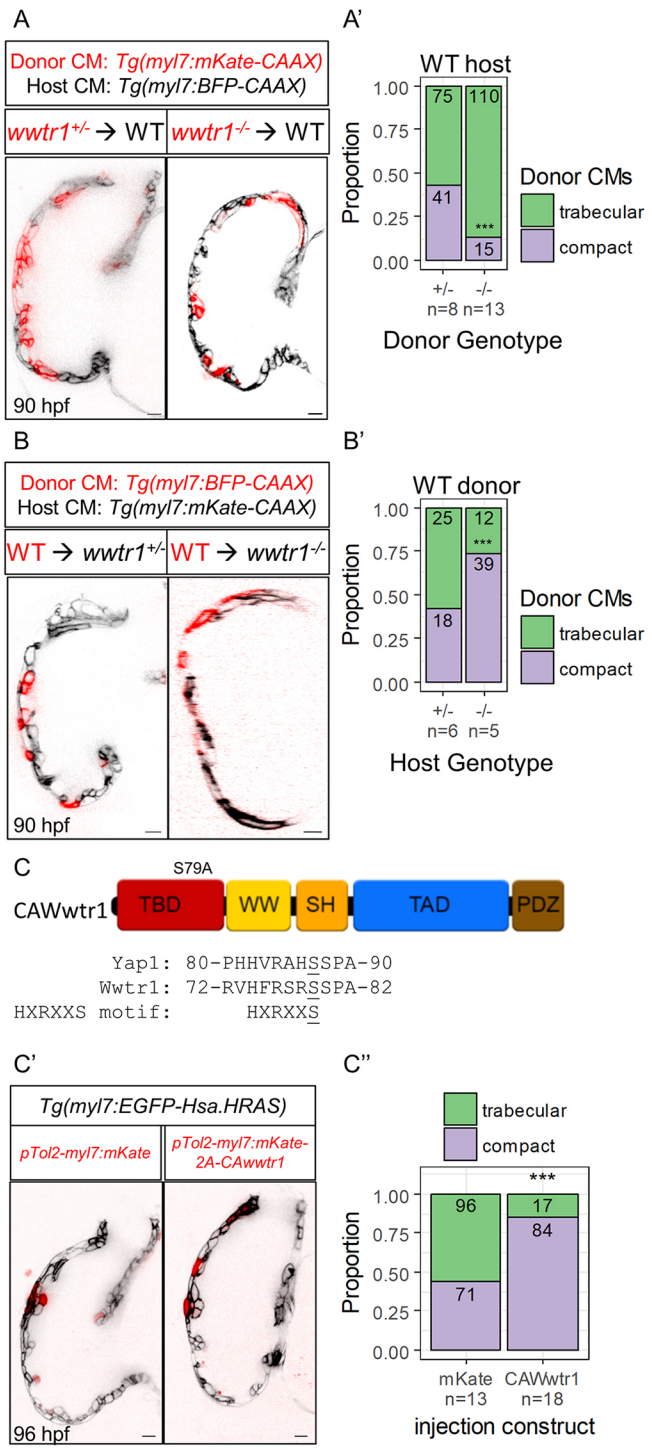

Fig. 4. Preference for *wwtr1* mutant cardiomyocytes to enter the trabecular layer in wild-type hearts. Confocal sagittal or transverse (WT→*wwtr1*$^{-/-}$) sections of mosaic hearts derived from transplanting *wwtr1*$^{+/-}$ or *wwtr1*$^{-/-}$ cells into wild-type hosts (A), and vice versa (B). Scale bars: 10 µm. (A′,B′) Proportion and number of donor cardiomyocytes contributing to the trabecular (green) or compact (purple) layers. Detailed quantification can be found in Fig. S6A,B. ***P<0.001 by exact Binomial test. (C) S79A substitution in Wwtr1 results in a constitutively active Wwtr1 protein (CAWwtr1). Peptide alignment of Wwtr1 to Yap1 surrounding the HXRXXS motif corresponding to S87 of Yap1. (C′) Confocal mid-sagittal sections of hearts from wild-type larvae injected with *myl7:mKate* (control) or *myl7:mKate-2A-CAwwtr1* plasmids. Scale bars: 10 µm. (C″) Proportion and number of cardiomyocytes positive for mKate or CAWwtr1 found in the trabecular (green) or compact (purple) layers. Detailed quantification can be found in Fig. S6C. ***P<0.001 by exact Binomial test.

57-59 hpf, just prior to the initiation of trabeculation. A total of 33 genes were significantly differentially regulated (Fig. S9A, Table S1). These genes can be grouped into different categories, including muscle, actomyosin network, Wnt signaling, metabolism, extracellular matrix (ECM), ECM degradation and others (Fig. S9B). Because of the architectural phenotypes of 52 hpf *wwtr1*$^{-/-}$ cardiomyocytes (Fig. 5), we focused our attention on differentially expressed genes that regulate the actomyosin network, including *myh10*, *mybphb* and *abraa* (Fig. S9C). These genes have been reported to be expressed in zebrafish hearts (Chong et al., 2012; Huang et al., 2013). Using whole-mount *in situ* hybridization (WISH), we found that *mybphb* is indeed expressed in most of the muscular tissues, including the heart, and that *wwtr1*$^{-/-}$ embryos exhibited heart-specific downregulation of *mybphb* expression (Fig. S9D), consistent with our RNAseq data. Myh10 has been shown to modulate cardiomyocyte morphology (Chopra et al., 2018), and to play important roles in heart development (Tullio et al., 1997). However, mosaic expression of *mybphb* and mouse *Myh10* in cardiomyocytes resulted in cardiomyocyte cell death (data not shown), precluding experiments using this strategy.

Neuregulin signaling and cardiac contractility regulate Wwtr1 cellular localization

To further analyze the role of Wwtr1 in cardiac trabeculation, we investigated its regulation by two pathways implicated in this process: the neuregulin and Notch signaling pathways. Overexpression of Nrg2a in cardiomyocytes resulted in the loss of nuclear enrichment of Wwtr1 immunostaining in these cells (Fig. 6A); however, the loss of *erbb2* did not modify the localization of Wwtr1 in cardiomyocytes (Fig. 6B). Additionally, loss of *jag2b*, which, as mentioned earlier, has been reported to be required for cardiomyocyte-specific *tp1* Notch reporter expression (Han et al., 2016), did not appear to affect the localization of Wwtr1 in cardiomyocytes (Fig. S10A). These results suggest that neuregulin signaling can modulate the localization of Wwtr1 in cardiomyocytes.

Cardiac contractility/blood flow has been shown to modulate cardiac trabeculation (Chi et al., 2008; Peshkovsky et al., 2011; Samsa et al., 2015), and these mechanical cues were shown in other systems to regulate YAP1 nucleo-cytoplasmic localization (Esteves de Lima et al., 2016; Nakajima et al., 2017). We found that defects in cardiac contractility, by using *tnnt2a* (*silent heart/sih*) and *myh6* (*weak atrium/wea*) morpholinos, resulted in aberrant accumulation of Wwtr1 in the cytoplasm of cardiomyocytes, although some nuclear localization could still be observed (Fig. S10B). Furthermore, we found that Wwtr1 immunostaining was now evident in the nuclei of atrial cardiomyocytes of *tnnt2a* and *myh6* morphant hearts. In these morphant animals, nuclei of endocardial cells also exhibited Wwtr1 immunostaining, but limited to the affected cardiac chambers (i.e. both cardiac chambers of *tnnt2a* morphants, and the atrium of *myh6* morphants) (Fig. S10B). Taken together, Wwtr1 localization appears to be modulated by neuregulin signaling and cardiac contractility.

DISCUSSION

The Hippo signaling pathway has been shown to regulate myocardial growth (Heallen et al., 2011; Xin et al., 2011; von Gise et al., 2012). In this study, we uncover novel functions for this pathway, especially for Wwtr1 during cardiac wall morphogenesis (Fig. 7).

Cardiac trabeculation initiates with cardiomyocyte delamination (Liu et al., 2010; Staudt et al., 2014) and, at least in mouse,

Development (2018) 145, dev159210. doi:10.1242/dev.159210

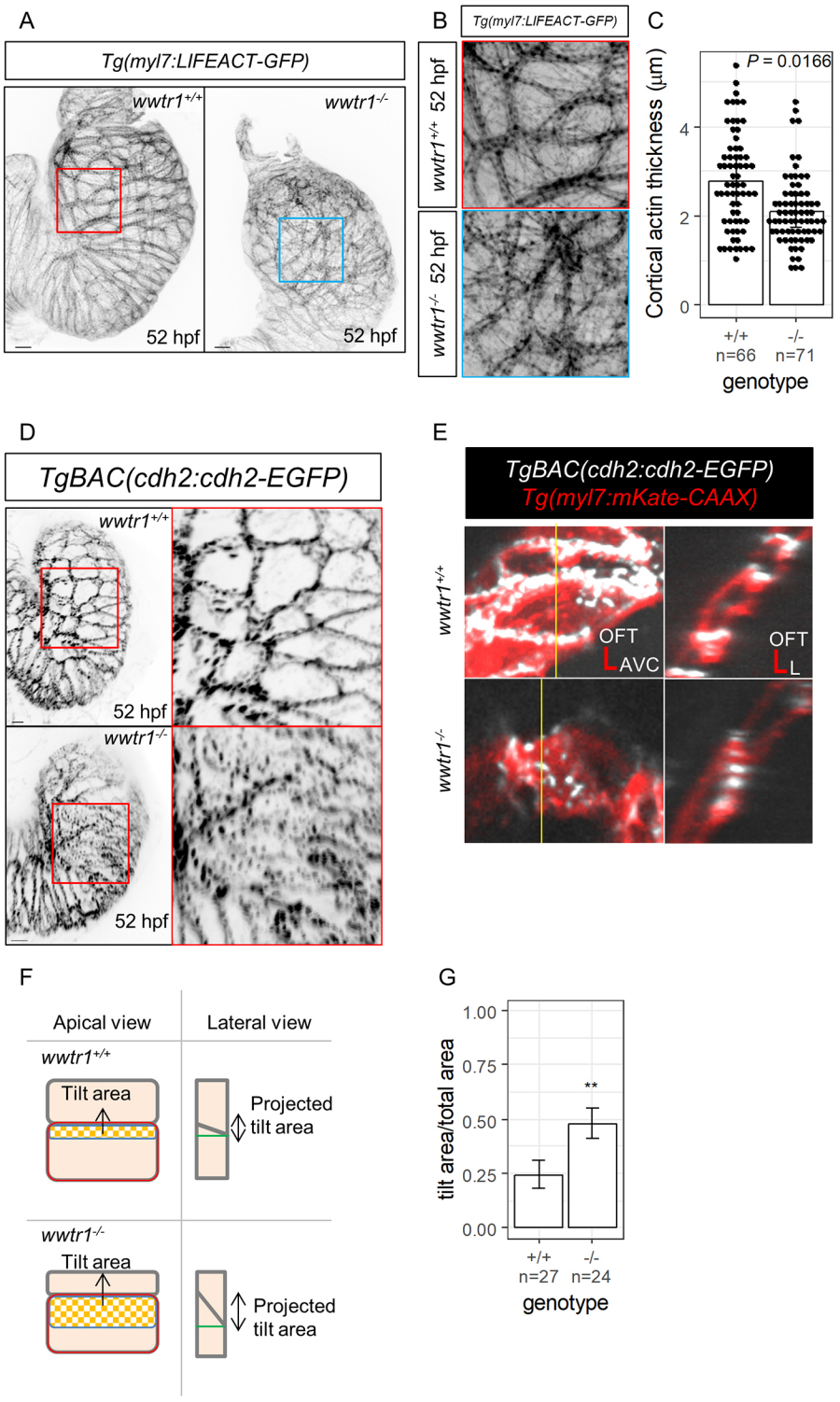

Fig. 5. Disruptions to the architecture of the compact wall myocardium in *wwtr1*$^{-/-}$ hearts. (A) Maximum intensity projections of 52 hpf zebrafish hearts showing the overall expression pattern of LIFEACT-GFP, which marks F-actin localization (8/8 *wwtr1*$^{+/+}$ and 6/7 *wwtr1*$^{-/-}$ hearts). Scale bars: 10 µm. (B) Apical views of cardiomyocytes corresponding to the area demarcated in their respective boxes in A. (C) Quantification of cortical actin thickness in ventricular cardiomyocytes. Each dot represents a cortical actin bundle (*n* cortical actin bundles were assessed from six *wwtr1*$^{+/+}$ and seven *wwtr1*$^{-/-}$ hearts). *P*-value was calculated using a two-sample *t*-test. (D) Maximum intensity projections of 52 hpf zebrafish hearts showing the distribution of N-cadherin-GFP in ventricular cardiomyocytes. Nine out of 11 *wwtr1*$^{+/+}$ hearts exhibit distinct N-cadherin-GFP localization to cardiomyocyte junctions, whereas 11/15 *wwtr1*$^{-/-}$ hearts exhibit punctate distribution of N-cadherin-GFP. Scale bars: 10 µm. (E) Apical views of cardiomyocytes and optical cross-section corresponding to the yellow vertical lines. The N-cadherin-GFP distribution in *wwtr1*$^{-/-}$ cardiomyocytes appears punctate along the cell junctions and the lateral contacts appear oblique to the apical surface (or 'tilted'). OFT, outflow tract; AVC, atrioventricular canal; L, lumen. (F) Schematic illustration of E and strategy to quantify the 'tilting' of lateral contacts. The rectangle outlined in red is the 'total area', whereas the inner rectangle outlined in blue is the 'tilt area'. The green horizontal line in the 'lateral view' is perpendicular to the apical surface. (G) Proportion of 'tilt area' to 'total area' of ventricular cardiomyocytes (*n*=total number of cardiomyocytes assessed from four hearts of each genotype). Error bars are one unit of standard deviation. ***P*<0.01 by two-sample *t*-test.

proliferation (Chen et al., 2004; Grego-Bessa et al., 2007). In our study, we found that *wwtr1*$^{-/-}$ hearts exhibit little to no appreciable mature trabecular ridges, fewer cardiomyocytes in the trabecular layer and a lower cardiomyocyte proliferation rate. In addition, we showed that wild-type cardiomyocytes are less frequently found in the trabecular layer of *wwtr1*$^{-/-}$ than *wwtr1*$^{+/-}$ mosaic hearts, indicating that the mutant cardiac wall cannot support trabeculation. Taken together, these results indicate that Wwtr1 has a role in cardiomyocyte development and proliferation during trabecular morphogenesis.

Signaling and mechanical cues regulate cardiomyocyte morphogenetic movements during trabeculation (Staudt et al., 2014). Neuregulin signaling is required to transform a single-layered ventricular wall into a mature trabeculated wall (Gassmann et al., 1995; Lee et al., 1995; Meyer and Birchmeier, 1995; Liu et al., 2010; Rasouli and Stainier, 2017). Here, we found that nuclei of

Development (2018) 145, dev159210. doi:10.1242/dev.159210

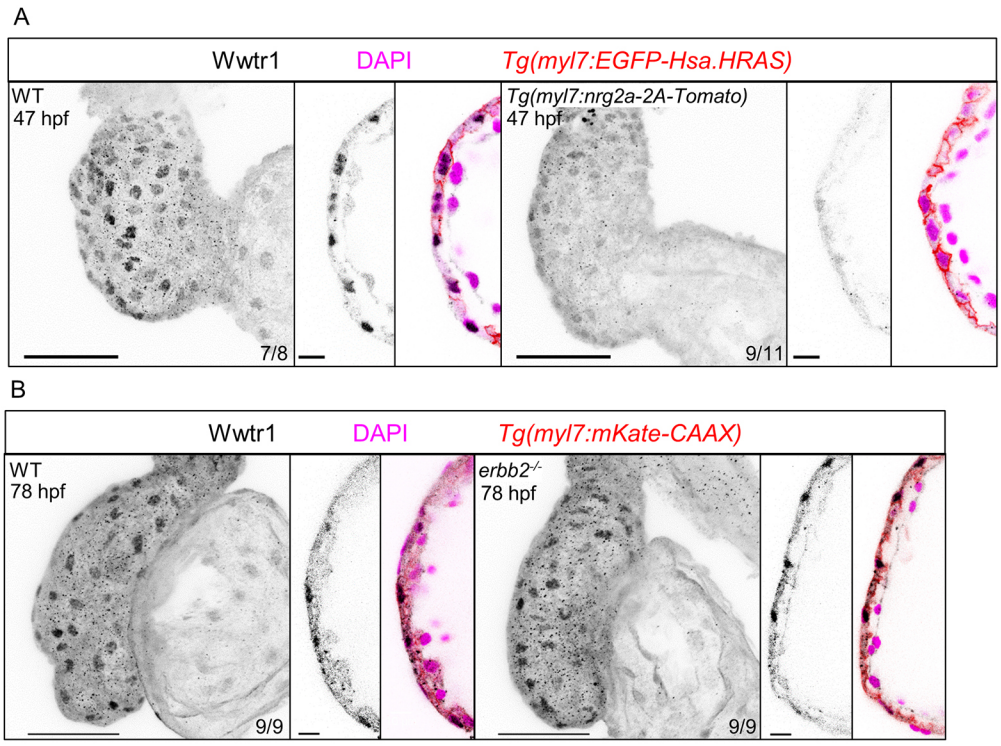

Fig. 6. Regulation of Wwtr1 localization by neuregulin signaling. (A) Maximum intensity projections of whole hearts and single confocal sections of the ventricular outer curvature at 47 hpf. Wwtr1 immunostaining was performed on *Tg(myl7:nrg2a-2A-Tomato)* embryos and their non-transgenic siblings as control (wild type). (B) Maximum intensity projections of whole hearts and single confocal sections of the ventricular outer curvature at 78 hpf. Wwtr1 immunostaining was performed on *erbb2* mutant larvae and their wild-type siblings. Scale bars: 50 µm; 10 µm (sections).

cardiomyocytes in the trabecular layer exhibit weaker nuclear expression of Wwtr1, possibly in response to Nrg2a stimulation. Moreover, our mosaic studies found that *wwtr1*$^{-/-}$ cardiomyocytes have a greater preference for the trabecular layer and, conversely, that CAWwtr1-expressing cardiomyocytes have a greater preference for the compact layer, indicating that Wwtr1 has a role in modulating the likelihood of a cardiomyocyte to enter the trabecular layer.

Although *nrg2a* appears to be expressed in all endocardial cells of the ventricular outer curvature (Rasouli and Stainier, 2017), only a subset of compact layer cardiomyocytes delaminate to become trabecular cardiomyocytes (Staudt et al., 2014). It is possible that, during this process, the delaminating cardiomyocytes, as they leave the epithelial sheet, mechanically impact their neighbors, a phenomenon that has been observed during cell extrusion and apoptosis in tissue development and morphogenesis (Toyama et al.,

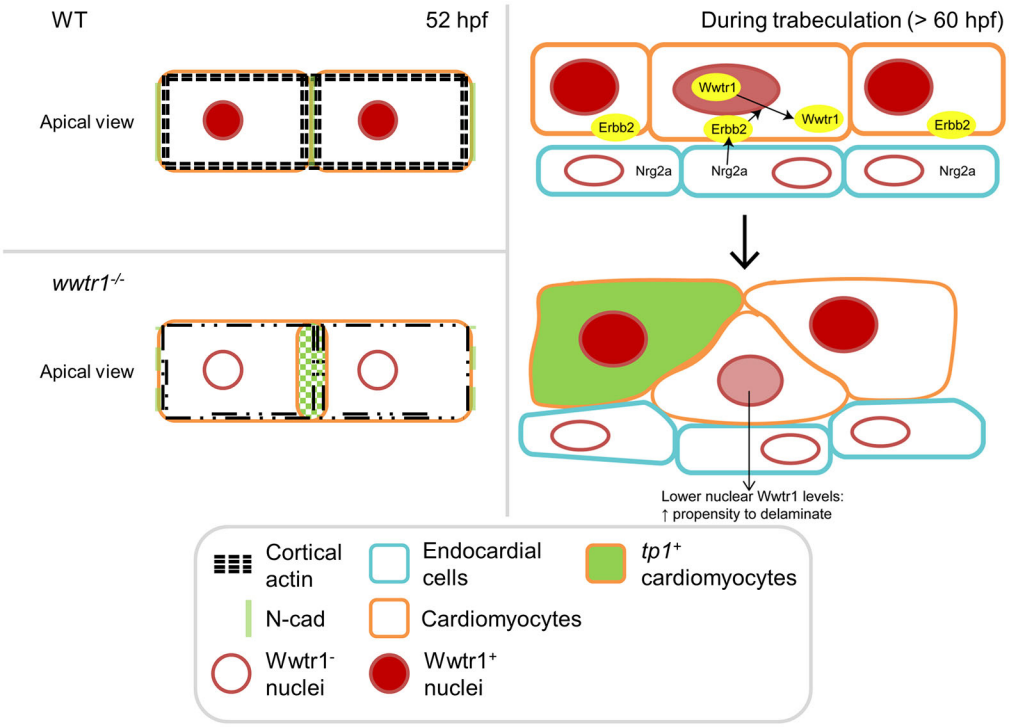

Fig. 7. Wwtr1 maintains compact wall architecture and also modulates trabeculation. Wwtr1 is required for compact wall architecture as its loss leads to disorganized cortical actin and abnormal cell-cell junctions. During trabeculation, cardiomyocytes in the compact wall contain varying levels of nuclear Wwtr1 protein, which appear to be negatively regulated by neuregulin signaling. Cardiomyocytes with lower nuclear Wwtr1 levels exhibit an increased propensity to delaminate and seed the trabecular layer. In compact wall cardiomyocytes, Wwtr1 also drives *tp1* Notch reporter expression in a cell-autonomous manner.

Development (2018) 145, dev159210. doi:10.1242/dev.159210

2008; Monier et al., 2015; Ambrosini et al., 2017). Specifically, single cells undergoing extrusion can affect the cellular tension of neighboring cells (Teng et al., 2017) and, moreover, these neighboring cells tend to exhibit nuclear localization of YAP1 (Saw et al., 2017), in keeping with the cytoskeletal tension-sensing property of YAP1/WWTR1 (Dupont et al., 2011). It is therefore possible that, during trabeculation, as individual cardiomyocytes delaminate to leave the compact wall, the mechanical influence on their neighbors induces Wwtr1 nuclear localization. In turn, Wwtr1 in compact layer cardiomyocytes cell-autonomously promotes *tp1* Notch reporter expression, the activity of which has been shown to be restricted to compact wall cardiomyocytes by lineage tracing (Jiménez-Amilburu et al., 2016).

Recent studies have implicated YAP1/WWTR1 in the regulation of the cytoskeletal network and cell-cell junctions through the transcription of genes that modulate them (Kim et al., 2017; Kimelman et al., 2017). We observed a downregulation of *myh10* and *mybphb* in 57-59 hpf *wwtr1*$^{-/-}$ hearts, which may underlie the cardiomyocyte architecture phenotypes (Fig. 5). Indeed, MYH10 has been shown to play crucial roles in cardiomyocyte adherens junction maintenance, sarcomere organization, ventricular septum development and outflow tract orientation (Tullio et al., 1997; Ma et al., 2009; Li et al., 2015). *MYBPH* (the human ortholog of *mybphb*), on the other hand, is strongly expressed in muscle (Gilbert et al., 1999; Hayashi et al., 2016); together with sarcomeric myosin heavy chain, it can induce assembly of F-actin cables in non-muscle cells (Welikson and Fischman, 2002). These two genes are also downregulated in *asb2b* mutant hearts, and *asb2b*, which encodes an E3 ubiquitin ligase, has been implicated in cardiomyocyte maturation (Fukuda et al., 2017) (Table S2). Moreover, *asb2b*$^{-/-}$ atrial cardiomyocytes, similar to *wwtr1*$^{-/-}$ ventricular cardiomyocytes, exhibit aberrant N-cadherin localization. However, *asb2b* is not differentially regulated in *wwtr1*$^{-/-}$ hearts, or vice versa (Table S2). These observations support the notion that Wwtr1, through the expression of *myh10* and *mybphb*, modulates cardiomyocyte cytoskeletal maturation, and suggest a possible cross-talk between Asb2b and Wwtr1 in this process.

The Hippo signaling pathway is known for its role in modulating myocardial growth (Heallen et al., 2011; Xin et al., 2011; von Gise et al., 2012) and regeneration (Xin et al., 2013b; Heallen et al., 2013). In mouse, deletion of *Yap1* in cardiac lineages (*Nkx2.5-Cre*) resulted in smaller hearts with thinner ventricular walls, but trabeculation did not appear to be affected (Xin et al., 2011). Although a *Wwtr1* mutant was studied to address the role of WWTR1 in cardiac growth (Xin et al., 2013b), a careful investigation into its role in cardiac trabeculation was not carried out. Nevertheless, it is interesting to note that mouse *Tead1* global mutants exhibit reduced cardiac trabeculation, which might be due to cardiomyocyte cell death, as indicated by the presence of 'ghost' particles detected by the periodic acid-Schiff staining (Chen et al., 1994). Additional studies will be required to determine the exact role of the Hippo pathway and its transcriptional effectors in cardiac trabeculation in mouse and in zebrafish.

MATERIALS AND METHODS

Ethics statement

All zebrafish husbandry was performed under standard conditions in accordance with institutional (Max Planck Society) and national ethical and animal welfare guidelines.

Transgenic and mutant zebrafish lines

Transgenic lines used in this study were: *Tg(myl7:mKate-CAAX)*^{sd11Tg} (Lin et al., 2012); *Tg(myl7:EGFP-Hsa.HRAS)*^{s883Tg} (D'Amico et al., 2007); *Tg(-5.1myl7:DsRed2-NLS)*^{f2Tg} (Rottbauer et al., 2002), abbreviated *Tg(myl7:nlsDsRed)*; *Tg(EPV.Tp1-Mmu.Hbb:Venus-Mmu.Odc1)*^{s940Tg} (Ninov et al., 2012), abbreviated *Tg(tp1:Venus-PEST)*; *Tg(myl7:BFP-CAAX)*^{bns193Tg} (this study); *Tg(myl7:LIFEACT-GFP)*^{s974Tg} (Reischauer et al., 2014); *TgBAC(cdh2:cdh2-EGFP,crybb1:ECFP)*^{zf517Tg} (Revenu et al., 2014), abbreviated *TgBac(cdh2:cdh2-EGFP)*; *Tg(-0.2myl7:EGFP-podocalyxin)*^{bns103Tg} (Jiménez-Amilburu et al., 2016), abbreviated *Tg(-0.2myl7:EGFP-podxl)*; *Tg(-0.2myl7:Mark3a-tagRFPt)*^{bns240Tg} (Jiménez-Amilburu et al., 2016); and *Tg(myl7:nrg2a202-p2a-tdTomato)*^{bns140Tg} (Rasouli and Stainier, 2017), abbreviated *Tg(myl7:nrg2a-2A-Tomato)*.

Mutant lines used in this study were: *erbb2*^{st61} (Lyons et al., 2005) and *jag2b*^{hu3425} (Han et al., 2016).

The *wwtr1*^{bns35} allele was identified from a CRISPR/CAS9-mediated mutagenesis. Single-guide RNA (sgRNA) (5′-TCACCACATGGCACGA-CCCC-3′) sequence was designed through the CRISPR design tool from the Zhang Lab (crispr.mit.edu). sgRNA DNA oligos were cloned into the pT7-gRNA vector (Addgene plasmid #46759). The vector was linearized with *Bsm*BI enzyme and followed by *in vitro* transcription with MEGAshortscript T7 transcription kit (Ambion) to obtain sgRNA for injections. *CAS9* mRNA was obtained by *in vitro* transcription of linearized pT3TS-nCas9n vector (Addgene plasmid #46757) with MEGAscript T3 transcription kit (Ambion). sgRNA (100 pg) and 150 pg of *CAS9* mRNA were co-injected into one-cell stage AB embryos. The *wwtr1*^{bns35} allele contains a 29 bp insertion. To genotype this allele, we used the following primers, 5′-TTT-GTTGTGCAGTCACATTGAG-3′ and 5′-GAGGGCGTCATGCTCTTC-3′, to generate 66 and 95 bp amplicons corresponding to wild-type and mutant alleles, respectively, which can be separated by gel electrophoresis on a 2% gel. When exogenous *wwtr1* was present, the following intron-specific primer, 5′-CTGGAAGGGTGTCCACTGAT-3′, was paired with the above-mentioned reverse primer, 5′-GAGGGCGTCATGCTCTTC-3′, which leads to 169 and 198 bp amplicons corresponding to wild-type and mutant alleles, respectively. These amplicons can be resolved by gel electrophoresis on a 2% gel. Most experiments were performed on embryos/larvae from incrossing F3 heterozygous parents, which themselves were generated by serial outcrosses. Some *wwtr1*^{bns35} mutants can survive to adulthood.

Morpholinos

Morpholinos used in this study were: *tnnt2a* (*silent heart* or *sih*) morpholino (Sehnert et al., 2002), *myh6* (*weak atrium* or *wea*) morpholino (Berdougo et al., 2003) and standard control morpholino (Gene Tools). A total of 1 ng of each morpholino was injected into one-cell stage embryos.

Plasmid constructs

The pTol2 *myl7:mKate* plasmid was generated by cloning the *Nhe*I-CCACC-mKate-*Xho*I fragment into a multiple cloning site (MCS) of a Tol2 enabled vector that is downstream of a *myl7* promoter. CCACC is the Kozak sequence. The pTol2 *myl7:mKate-2A-wwtr1* plasmid was generated by ligating the *Nhe*I-CCACC-mKate-*Eco*RI, *Eco*RI-2A-*Cla*I and *Cla*I-wwtr1-*Xho*I fragments and cloned into the MCS of the aforementioned Tol2 enabled vector. The 2A peptide sequence is GSGEGRGSLLTCGDVEENPGP (Kim et al., 2011). To obtain the WW*, TBD* and ΔTBD mutant constructs, site-directed mutagenesis (SDM) was performed using a Q5 Site-Directed Mutagenesis Kit (NEB #E0552S) on the pTol2 *myl7:mKate-2A-wwtr1* plasmid. The following primers were used for site-directed mutagenesis: WW*, 5′-GACgctAGGAAGAGCATGACGCCC-3′ and 5′-GTGagcTGT-GGTGATCTTCTCAATGTGATTG-3′; TBD*, 5′-TATGCCGCAGgctTT-CTTCCAGG-3′ and 5′-TCCTTGTTCCTCCAGGAGC-3′; ΔTBD, 5′-TCCGGTTCTCTCCCGCCG-3′ and 5′-CATATCCTTGTTCCTCCAG-GAGCTC-3′. Lowercase letters are codons corresponding to amino acid substitutions to alanine. All reactions were carried out following the manufacturer's recommendation. The mutated *wwtr1* constructs were confirmed by Sanger sequencing and re-cloned using the *Cla*I and *Xho*I cloning sites into the parent plasmid to avoid any off-target mutations. The CAWwtr1 construct was obtained by SDM via PCR with the following primers: 5′-GAGCCCGCCGGCAGCTGTAGGGACGCCGGAGAagcGCGCGAGC-GAAAG-3′ and 5′-ACAGCTGCCGGCGGGCTCCGTG-3′ [the underlined sequence indicates the *Nae*I restriction sites and lowercase letters are the

Development (2018) 145, dev159210. doi:10.1242/dev.159210

codon for the alanine substitution (S79A)]. The amplicon was digested and cloned into the pTol2 *myl7:mKate-2A-wwtr1* plasmid. Correct orientation of the insert was selected by Sanger sequencing. pTol2 *myl7:mKate-2A-mybphb* plasmid was generated by replacing *wwtr1* from pTol2 *myl7:mKate-2A-wwtr1* with zebrafish *mybphb*. pTol2 *myl7:mKate-2A-Myh10* was generated in a similar manner, but with mouse *Myh10*. The injection cocktail consisted of 15 pg of *transposase* mRNA and 8-12 pg of vector.

Confocal microscopy

Embryos at 1 day post fertilization (dpf) were grown in embryo media containing phenylthiourea (PTU) to prevent pigmentation. Live embryos or larvae were embedded in 1% low-melt agarose (LMA) dissolved in egg media containing 0.2% (w/v) tricaine on glass-bottomed dishes. Zeiss Spinning Disk or LSM800 (inverted) confocal microscopes were used. Hearts were manually isolated from fixed animals and embedded in 1% LMA dissolved in 1× PBS on glass-bottomed dishes.

Fixed samples preparation

Embryos or larvae were first anesthetized with 0.2% tricaine for up to 5 min followed by fixation with 4% PFA. Samples were fixed for at least 2 h at room temperature or overnight at 4°C. For immunostaining, fixed samples were decapitated, leaving the hearts attached to the head and clearing out any residual yolk. The remaining body was used for genotyping, if applicable. Images for Fig. 5A,B, Fig. S7C,D were obtained from isolated fixed hearts.

Whole-mount immunostaining

Fixed samples were washed for 30 min with 1× PBSTTD [1× PBS, 0.1% Tween-20, 0.1% Triton X-100 and 1% DMSO (or 2% DMSO when using D24E4 primary antibody)]. This wash was followed by 1 h blocking with 2 mg ml^{-1} BSA and 5% sheep serum added to 1× PBSTTD. Primary antibodies were diluted (see below) in blocking solution and incubated with samples overnight at 4°C. After incubation with primary antibody(ies), samples were rinsed three times with 1× PBSTTD and then washed every 30 min with 1×PBSTTD for at least 6 h. This step was followed by secondary antibody incubation overnight at 4°C and a similar washing regimen the next day. Samples were post-fixed with 4% PFA for at least 20 min prior to confocal imaging. Primary antibodies used and their dilutions were: Wwtr1 (Cell Signaling, D24E4), 1:200; pMRLC (Abcam, ab2480), 1:100; and MF20 (Developmental Studies Hybridoma Bank; DSHB), 1:200. All secondary antibodies were obtained from Life Technologies and used at 1:500. Phalloidin conjugated to Alexa-568 (Life Technologies) was used at 1:500 and DAPI (Life Technologies) at 1:10,000. Endogenous transgenic fluorescent signal perdured through the procedures and no further antibody staining was required. When staining mutant samples, wild-type and mutant samples were placed in the same reaction tube. For morpholino experiments, control and *tnnt2a* or *myh6* morphants were placed in the same reaction tube. Control morphants retained most of the trunk (see 'Fixed samples preparation') for easy identification.

Whole-mount *in situ* hybridization

Standard whole-mount in situ hybridization protocol was carried out (Thisse and Thisse, 2008). Primers to make the *mybphb* antisense probe used in this study were: 5′-CATTAACCCTCACTAAAGGGAAATGCCGGCAAAA-CCAGC-3′ and 5′-TAATACGACTCACTATAGGGGATCTTCACGGA-GGCAG-3′. cDNA from adult zebrafish hearts was used as a template for the PCR reaction. Purified amplicons were used as a template for the *in vitro* transcription (T7 promoter) reaction to obtain the antisense probe. At day 3 of the whole-mount in situ hybridization protocol, after development of the alkaline phosphatase (AP) staining, samples were fixed with 4% PFA for at least 20 min followed by three washes with 1× PBSTTD. This step was followed by the whole-mount immunostaining protocol with the MF20 primary antibody. Images were obtained with Nikon SMZ25 stereomicroscopes. Samples were mounted on a 1% LMA (dissolved in 1× PBS) scaffold. Mutants and wild-type siblings were placed in the same reaction tube.

Image analyses

Image analyses were carried out in Imaris (Bitplane), Zen Blue (Zeiss) or Fiji (Schindelin et al., 2012). Details for image analyses can be found in their individual subsections.

Statistical analyses

Analyses were carried out in R. The packages used for data management and plotting were *ggplot2* (Wickham, 2010), *beeswarm*, *RColorBrewer* and *plyr*. Poisson regression statistical test was used on count data, otherwise standard linear models (i.e. Student's *t*-test, linear regression, etc.) were used on continuous data. Distribution of cardiomyocytes between compact and trabecular layer was tested with the Binomial test, setting the controls as the null hypothesis parameter. Data and scripts are available upon request from the authors.

Transplantation

Mutant and heterozygous embryos were obtained from a cross between *wwtr1*$^{-/-}$; *Tg(myl7:mKate-CAAX)* (♂) and *wwtr1*$^{+/-}$; *Tg(tp1:Venus-PEST)* (♀). Wild-type embryos were obtained from a cross between *Tg(myl7:BFP-CAAX)* and *Tg(tp1:Venus-PEST)*. Donors were kept alive to screen for presence of the transgenes as well as for genotyping (when applicable). Both transgenes must be present in donors, but only the *Tg(tp1:Venus-PEST)* transgene was needed in hosts. When analyzing distribution of donor cardiomyocytes between compact and trabecular layer (Fig. 4A,B), only the *myl7* transgenics were examined.

Wwtr1 expression analyses

Images were acquired on a Spinning Disk microscope and analyzed with Imaris. Individual nuclei were selected using the Surface creation tool on the DAPI channel. Nuclei of trabecular cardiomyocytes were manually selected, as well as nuclei of adjacent compact layer cardiomyocytes. These cardiomyocytes could be identified with the aid of the *Tg(myl7:mKate-CAAX)* marker. The average intensity of Wwtr1 channel was extracted and analyzed in R.

Analyzing trabecular cardiomyocytes

Images were acquired on a Spinning Disk microscope and processed in Imaris. To obtain surface reconstruction of the *Tg(myl7:EGFP-Hsa.HRAS)* signal, we used the Normal Shading function in Volume tool. To determine the total number of ventricular cardiomyocytes, we used *Tg(myl7:EGFP-Hsa.HRAS)* in conjunction with *Tg(myl7:nlsDsRed)*. The same animal was followed for all three time points: 58, 72 and 96 hpf. All nuclei were selected with the 'Spot Creation' tool. Cardiomyocytes in the atrium, atrio-ventricular canal (AVC) and outflow tract were manually excluded. For simplicity, a binary assignment of ventricular cardiomyocytes was made: 'Compact wall cardiomyocytes' was defined as the outermost layer of cardiomyocytes, otherwise cardiomyocytes were assigned to 'Trabecular cardiomyocytes'.

Mosaic analyses of trabecular cardiomyocyte morphology were carried out by injecting the pTol2 *myl7:mKate* plasmid into one-cell stage embryos from an incross of *wwtr1*$^{+/-}$ fish. Trabecular cardiomyocytes expressing mKate were selected with the 'Surface Creation' tool to apply channel masking on the LIFEACT-GFP channel.

Analyzing myocardial *tp1* activity

Images were acquired on a Spinning Disk microscope and analyzed with Imaris. Maximum intensity projections were made to count the number of cardiomyocytes that express the *tp1* Notch reporter. To test which domain of Wwtr1 was required for myocardial *tp1* Notch reporter expression, the various Wwtr1 constructs were injected into one-cell stage embryos from an incross of *wwtr1*$^{+/-}$ animals. *tp1*$^{+}$ mutant hearts were hearts that showed at least one double-labeled *tp1*$^{+}$, mKate^{+} cardiomyocyte, otherwise assigned as *tp1*$^{-}$. For transplantation experiments, we relied on the donor/host cardiomyocyte marker to assign *tp1*$^{+}$ donor/host cardiomyocytes. As donor animals were pre-screened for the presence of transgenes both marking cardiomyocytes and reporting *tp1* activity, we could infer whether a *tp1*$^{+}$ cardiomyocyte belonged to the host if the host cardiomyocyte marker was absent.

Quantifying cardiomyocyte distribution between compact and trabecular layers

As the transplant and the mosaic CAWwtr1 experiments lacked a nuclear marker, the strategy to quantify the number of cardiomyocytes in the compact versus the trabecular layer had to be modified. As cardiomyocytes

Development (2018) 145, dev159210. doi:10.1242/dev.159210

expressed transgenes that mark the membranes (EGFP-Hsa.HRAS, mKate-CAAX or BFP-CAAX), we carefully classified outer-curvature ventricular cardiomyocytes as 'compact layer' or 'trabecular layer' through the *z*-stacks. 'Compact layer' cardiomyocytes were those in the outermost layer, otherwise classified as 'trabecular layer'.

Cortical actin thickness

Images were acquired with a Spinning Disk microscope and analyzed on Fiji. A background subtraction was applied on the LIFEACT-GFP channel using a 30 pixel rolling ball radius. A maximum intensity projection was generated followed by an automatic binary threshold of the gray values. We drew lines perpendicular to the cortical actin, sampling across the whole ventricular outer curvature wall, to generate a kymograph for calculation of cortical actin thickness.

'Tilting' extent of cardiomyocytes

Images were acquired with a Spinning Disk microscope and analyzed using Fiji. First, a maximum intensity projection of the mKate-CAAX (cardiomyocyte membranes) and N-cadherin-GFP channels was generated separately. Cardiomyocyte membranes were manually drawn on the mKate-CAAX channel to demarcate individual cells as a region of interest (ROI) and to calculate the 'total area'. The ROI was then applied on the N-cadherin-GFP channel to guide selection of the 'tilt area' (see Fig. 5F for schematic).

RNA-sequencing (RNAseq)

Embryos from an incross of *wwtr1*$^{+/-}$ fish were grown to 48 hpf. The fin-fold of these embryos were dissected out for genotyping. Wild-type and mutant siblings were identified and placed into separate dishes. Hearts were isolated starting from 57 hpf, for over a maximum of 2 h. Collections were made over five separate occasions to obtain 23 hearts per biological replicate (3 wild-type and mutant biological replicates each). Collection order was randomized over the genotype and biological replicates, and was never identical between collection sessions. Embryos were dissected in 1× Modified Barth's Saline (MBS). A 5× MBS solution consisted of: 17.6 ml 5 M NaCl, 1 ml 1 M KCl, 0.25 g $MgSO_4$, 1.2 g HEPES and 0.2 g $NaHCO_3$ to a final volume of 200 ml and adjusted to pH 7.8 with NaOH. The 1× MBS working solution consisted of: 20 ml of 5× MBS and 7 ml 0.1 M $CaCl_2$ adjusted to a final volume of 100 ml (protocol provided by David Kimelman, University of Washington, Seattle, WA, USA). Isolated hearts were snap frozen in liquid nitrogen and stored overnight at −80°C. Qiazol solution (Qiagen) was added followed by pipetting to mechanically dissociate the tissue. The samples were then passed through a QIAshredder homogenizer column (Qiagen) followed by RNA extraction with a miRNeasy micro kit (Qiagen). In-column DNase digestion was performed to eliminate DNA contamination. RNA and library preparation integrity were verified with a BioAnalyzer 2100 (Agilent) or LabChip G×Touch 24 (Perkin Elmer). Total RNA (6.5 ng) was used as input for Pico Input Mammalian (Takara Clontech). Sequencing was performed on the NextSeq500 instrument (Illumina) using v2 chemistry, resulting in a minimum of 30 M reads per library with a 1×75 bp single-end setup. The resulting raw reads were assessed for quality, adapter content and duplication rates with FastQC (www.bioinformatics.babraham.ac.uk/projects/fastqc). Reaper version 13-100 was employed to trim reads after a quality drop below a mean of Q20 in a window of 10 nucleotides (Davis et al., 2013). Only reads between 30 and 75 nucleotides in length were cleared for further analyses. Trimmed and filtered reads were aligned against the Ensembl Zebrafish genome version DanRer10 (GRCz10.87) using STAR 2.4.0a with the parameter '–outFilterMismatchNoverLmax 0.1' to increase the maximum ratio of mismatches to mapped length to 10% (Dobin et al., 2013). The number of reads aligning to genes was counted with the featureCounts 1.4.5-p1 tool from the Subread package (Liao et al., 2014). Only reads mapping at least partially inside exons were admitted and aggregated per gene. Reads overlapping multiple genes or aligning to multiple regions were excluded. Differentially expressed genes were identified using DESeq2 version 1.62 (Love et al., 2014). Only genes with a combined minimum mean of five reads were used for subsequent analyses. The Ensembl annotation was enriched with UniProt data (release 24.03.2017) based on Ensembl gene identifiers [Activities at the Universal Protein Resource (UniProt)]. Genes were classified in four groups by the following thresholds: significantly differentially expressed, ±1.0 $\log_2$FC (fold-change) and adjusted P<0.05; moderately differentially expressed, adjusted P<0.05; not significantly differentially expressed, ±1.0 $\log_2$FC; and not differentially expressed otherwise.

pMRLC immunostaining analysis

Images were acquired on a LSM800 (inverted) microscope with fixed settings and analyzed using Fiji. A maximum intensity projection of pMRLC and phalloidin channels was generated using the same settings for all samples. The outline of the ventricular chamber was manually drawn to obtain the average and median gray values of pMRLC and phalloidin. The mean/median gray values of pMRLC was divided by the mean/median gray values of phalloidin for each heart. These normalized values were used for analyses.

Podxl localization analysis

Hearts were imaged with a Spinning Disk microscope and analyzed using Zen Blue software. We analyzed 20 µm of sagittal sections surrounding the mid-sagittal plane. Each section was 1 µm. The method to quantify apical constriction was performed as described previously (Jiménez-Amilburu et al., 2016). To quantify the number of polarized and depolarized trabecular cardiomyocytes, we analyzed 26 µm of sagittal sections surrounding the mid-sagittal plane. Each section was 1 µm. Trabecular cardiomyocytes must not be in contact with the abluminal surface throughout the sections. Only trabecular cardiomyocytes that exhibited clear expression of EGFP-Podxl were assessed. They were counted as polarized if EGFP-Podxl was localized to the apical surface only and depolarized if EGFP-Podxl was distributed around the cell.

EdU labeling and quantification

Larvae (80 hpf) from *wwtr1*$^{+/-}$ incrosses were incubated with 1 mM EdU for 16 h in egg water containing PTU and 1% DMSO to facilitate EdU incorporation. Larvae were rinsed twice in egg water, anaesthetized with tricaine 0.4% (w/v) and fixed overnight with 4% PFA. Whole-mount immunostaining was performed as described previously (Inoue and Wittbrodt, 2011). Anti-DsRed (Clontech 632496; 1:300) and anti-GFP (Aves GFP-1020; 1:500) antibodies were used to label the *myl7*:nlsDsRed and *myl7*:EGFP-Hsa.HRAS reporter lines, respectively. The CLICK-IT (Invitrogen) reaction for EdU staining was performed by following the manufacturer's instructions. Images were acquired with Zeiss LSM800 confocal microscopy using a 40× [1.1 numerical aperture (NA)] water-immersion objective. EdU$^+$ cardiomyocytes and DsRed$^+$ cells were quantified by hand in the outer curvature of the cardiac ventricle. A line along the long axis of the cardiac ventricle was drawn to define the outer curvature of the ventricle and 24 planes were analyzed around the mid-sagittal plane, as described previously (Jiménez-Amilburu et al., 2016). The total number of DsRed$^+$ cells in the ventricle was quantified using Imaris. We performed this experiment twice independently.

Quantification of cardiac contraction and heart rate

Embryos (52 hpf) expressing the *myl7:EGFP-Hsa.HRAS* transgene were embedded in 1% LMA. Tricaine use was avoided throughout the procedure. The embryos were imaged live with a Spinning Disk confocal microscope with a 40× objective. The acquisition rate was set at 10 ms per frame. Movies of both GFP and bright-field channels were acquired (Movie 1). Movies from the GFP channel were used to quantify the heart rate using ImageJ software. First, the movies were loaded into ImageJ as a stack (time as the third dimension). The stack was 'resliced' with the following parameters: 'Start at-Right'; 'Rotate 90°'. Other parameters were left in their default settings. The resulting stack produces a kymograph that was converted into a binary image. The distance between two peaks is the duration of a single cardiac cycle. This distance was then converted into actual time scale (using the actual average number of frames per second recorded by Zen software during acquisition) in order to calculate the average number of heart beats per minute.

Movies from the bright-field channel were used to measure the ventricular fractional shortening with ImageJ (Hoage et al., 2012). Briefly, the maximum (end diastole) and minimum (end systole) short axis of the ventricle were measured from beating hearts to obtain the fractional shortening values=1-minimum/maximum.

Acknowledgements
We thank Felix Gunawan for an excellent immunostaining protocol; the trabeculation team, consisting of V.U., V.J.-A., Sven Reischauer, Rashmi Priya, Javad Rasouli and Pourya Savari, for discussions; Suchit Ahuja for injecting the *myl7:BFP-CAAX* construct; Hyun-Taek Kim for mouse *Myh10* plasmid for cloning; Viola Graef for critical reading of the manuscript; Rita Retzloff and team for zebrafish care; Michael Potente (MPI-HLR), Ong Yu-Ting (MPI-HLR), Shuichi Watanabe (MPI-HLR), Anna Romão Stone (MPI-HLR), Virginie Lecaudey (Frankfurt), Chaitanya Dingare (Frankfurt), Brian Link (Medical College of Wisconsin) and Joel Miesfeld (UC Davis) for sharing reagents and discussions on the Hippo signaling pathway; and Evan Tan (Singapore) for encouraging J.K.H.L. to generate a zebrafish *wwtr1* mutant. J.K.H.L. was a graduate student registered with the Faculty of Biological Sciences at Goethe University, Frankfurt am Main, Germany. Some data from this manuscript form part of J.K.H.L.'s PhD thesis submitted to Goethe University, Frankfurt am Main, Germany in 2018.

Competing interests
The authors declare no competing or financial interests.

Author contributions
Conceptualization: J.L., D.S.; Methodology: J.L., M.M.C., V.U., V.J., S.G., H.M.; Software: J.L., S.G.; Validation: J.L., M.M.C., V.U., D.S.; Formal analysis: J.L., V.U., S.G., D.S.; Investigation: J.L., M.M.C., V.U., S.G., H.M.; Resources: V.J., S.G., H.M., D.S.; Data curation: J.L., S.G.; Writing - original draft: J.L.; Writing - review & editing: J.L., M.M.C., V.U., V.J., D.S.; Visualization: J.L., V.U.; Supervision: D.S.; Project administration: D.S.; Funding acquisition: D.S.

Funding
This work was supported in part by funds from the Max-Planck-Gesellschaft.

Data availability
RNAseq data have been deposited in GEO under accession number GSE103169.

Supplementary information
Supplementary information available online at
http://dev.biologists.org/lookup/doi/10.1242/dev.159210.supplemental

References
Ambrosini, A., Gracia, M., Proag, A., Rayer, M., Monier, B. and Suzanne, M. (2017). Apoptotic forces in tissue morphogenesis. *Mech. Dev.* **144**, 33-42.
Berdougo, E., Coleman, H., Lee, D. H., Stainier, D. Y. R. and Yelon, D. (2003). Mutation of weak atrium/atrial myosin heavy chain disrupts atrial function and influences ventricular morphogenesis in zebrafish. *Development* **130**, 6121-6129.
Bersell, K., Arab, S., Haring, B. and Kühn, B. (2009). Neuregulin1/ErbB4 signaling induces cardiomyocyte proliferation and repair of heart injury. *Cell* **138**, 257-270.
Chen, Z., Friedrich, G. A. and Soriano, P. (1994). Transcriptional enhancer factor 1 disruption by a retroviral gene trap leads to heart defects and embryonic lethality in mice. *Genes Dev.* **8**, 2293-2301.
Chen, H., Shi, S., Acosta, L., Li, W., Lu, J., Bao, S., Chen, Z., Yang, Z., Schneider, M. D., Chien, K. R. et al. (2004). BMP10 is essential for maintaining cardiac growth during murine cardiogenesis. *Development* **131**, 2219-2231.
Cherian, A. V., Fukuda, R., Augustine, S. M., Maischein, H.-M. and Stainier, D. Y. R. (2016). N-cadherin relocalization during cardiac trabeculation. *Proc. Natl. Acad. Sci. USA* **113**, 7569-7574.
Chi, N. C., Shaw, R. M., Jungblut, B., Huisken, J., Ferrer, T., Arnaout, R., Scott, I., Beis, D., Xiao, T., Baier, H. et al. (2008). Genetic and physiologic dissection of the vertebrate cardiac conduction system. *PLoS Biol.* **6**, e109.
Chong, N. W., Koekemoer, A. L., Ounzain, S., Samani, N. J., Shin, J. T. and Shaw, S. Y. (2012). STARS is essential to maintain cardiac development and function in vivo via a SRF pathway. *PLoS ONE* **7**, e40966.
Chopra, A., Kutys, M. L., Zhang, K., Polacheck, W. J., Sheng, C. C., Luu, R. J., Eyckmans, J., Hinson, J. T., Seidman, J. G., Seidman, C. E. et al. (2018). Force generation via β-cardiac myosin, titin, and α-actinin drives cardiac sarcomere assembly from cell-matrix adhesions. *Dev. Cell* **44**, 87-96.e5.
Cox, A. G., Hwang, K. L., Brown, K. K., Evason, K., Beltz, S., Tsomides, A., O'Connor, K., Galli, G. G., Yimlamai, D., Chhangawala, S. et al. (2016). Yap reprograms glutamine metabolism to increase nucleotide biosynthesis and enable liver growth. *Nat. Cell Biol.* **18**, 886-896.
D'Amato, G., Luxán, G., del Monte-Nieto, G., Martínez-Poveda, B., Torroja, C., Walter, W., Bochter, M. S., Benedito, R., Cole, S., Martinez, F. et al. (2016). Sequential Notch activation regulates ventricular chamber development. *Nat. Cell Biol.* **18**, 7-20.
D'Amico, L., Scott, I. C., Jungblut, B. and Stainier, D. Y. R. (2007). A mutation in zebrafish hmgcr1b reveals a role for isoprenoids in vertebrate heart-tube formation. *Curr. Biol.* **17**, 252-259.
Davis, M. P. A., van Dongen, S., Abreu-Goodger, C., Bartonicek, N. and Enright, A. J. (2013). Kraken: a set of tools for quality control and analysis of high-throughput sequence data. *Methods* **63**, 41-49.
Dobin, A., Davis, C. A., Schlesinger, F., Drenkow, J., Zaleski, C., Jha, S., Batut, P., Chaisson, M. and Gingeras, T. R. (2013). STAR: ultrafast universal RNA-seq aligner. *Bioinformatics* **29**, 15-21.
Dupont, S., Morsut, L., Aragona, M., Enzo, E., Giulitti, S., Cordenonsi, M., Zanconato, F., Le Digabel, J., Forcato, M., Bicciato, S. et al. (2011). Role of YAP/TAZ in mechanotransduction. *Nature* **474**, 179-183.
D'Uva, G., Aharonov, A., Lauriola, M., Kain, D., Yahalom-Ronen, Y., Carvalho, S., Weisinger, K., Bassat, E., Rajchman, D., Yifa, O. et al. (2015). ERBB2 triggers mammalian heart regeneration by promoting cardiomyocyte dedifferentiation and proliferation. *Nat. Cell Biol.* **17**, 627-638.
Esteves de Lima, J., Bonnin, M.-A., Birchmeier, C. and Duprez, D. (2016). Muscle contraction is required to maintain the pool of muscle progenitors via YAP and NOTCH during fetal myogenesis. *Elife* **5**, e15593.
Fukuda, R., Gunawan, F., Beisaw, A., Jimenez-Amilburu, V., Maischein, H.-M., Kostin, S., Kawakami, K. and Stainier, D. Y. R. (2017). Proteolysis regulates cardiomyocyte maturation and tissue integration. *Nat. Commun.* **8**, 14495.
García-Rivello, H., Taranda, J., Said, M., Cabeza-Meckert, P., Vila-Petroff, M., Scaglione, J., Ghio, S., Chen, J., Lai, C., Laguens, R. P. et al. (2005). Dilated cardiomyopathy in Erb-b4-deficient ventricular muscle. *Am. J. Physiol. Heart Circ. Physiol.* **289**, H1153-H1160.
Gassmann, M., Casagranda, F., Orioli, D., Simon, H., Lai, C., Klein, R. and Lemke, G. (1995). Aberrant neural and cardiac development in mice lacking the ErbB4 neuregulin receptor. *Nature* **378**, 390-394.
Gilbert, R., Cohen, J. A., Pardo, S., Basu, A. and Fischman, D. A. (1999). Identification of the A-band localization domain of myosin binding proteins C and H (MyBP-C, MyBP-H) in skeletal muscle. *J. Cell Sci.* **112**, 69-79.
Grego-Bessa, J., Luna-Zurita, L., del Monte, G., Bolós, V., Melgar, P., Arandilla, A., Garratt, A. N., Zang, H., Mukouyama, Y.-S., Chen, H. et al. (2007). Notch signaling is essential for ventricular chamber development. *Dev. Cell* **12**, 415-429.
Han, P., Bloomekatz, J., Ren, J., Zhang, R., Grinstein, J. D., Zhao, L., Burns, C. G., Burns, C. E., Anderson, R. M. and Chi, N. C. (2016). Coordinating cardiomyocyte interactions to direct ventricular chamber morphogenesis. *Nature* **534**, 700-704.
Haskins, J. W., Nguyen, D. X. and Stern, D. F. (2014). Neuregulin 1-activated ERBB4 interacts with YAP to induce Hippo pathway target genes and promote cell migration. *Sci. Signal.* **7**, ra116.
Hayashi, S., Manabe, I., Suzuki, Y., Relaix, F. and Oishi, Y. (2016). Klf5 regulates muscle differentiation by directly targeting muscle-specific genes in cooperation with MyoD in mice. *Elife* **5**, e17462.
Heallen, T., Zhang, M., Wang, J., Bonilla-Claudio, M., Klysik, E., Johnson, R. L. and Martin, J. F. (2011). Hippo pathway inhibits Wnt signaling to restrain cardiomyocyte proliferation and heart size. *Science* **332**, 458-461.
Heallen, T., Morikawa, Y., Leach, J., Tao, G., Willerson, J. T., Johnson, R. L. and Martin, J. F. (2013). Hippo signaling impedes adult heart regeneration. *Development* **140**, 4683-4690.
Hilman, D. and Gat, U. (2011). The evolutionary history of YAP and the hippo/YAP pathway. *Mol. Biol. Evol.* **28**, 2403-2417.
Hoage, T., Ding, Y. and Xu, X. (2012). Quantifying cardiac functions in embryonic and adult zebrafish. *Methods Mol. Biol.* **843**, 11-20.
Huang, J., Wu, S., Barrera, J., Matthews, K. and Pan, D. (2005). The Hippo signaling pathway coordinately regulates cell proliferation and apoptosis by inactivating Yorkie, the Drosophila Homolog of YAP. *Cell* **122**, 421-434.
Huang, Y., Wang, X., Wang, X., Xu, M., Liu, M. and Liu, D. (2013). Nonmuscle myosin II-B (myh10) expression analysis during zebrafish embryonic development. *Gene Expr. Patterns* 13, 265-270.
Inoue, D. and Wittbrodt, J. (2011). One for all–a highly efficient and versatile method for fluorescent immunostaining in fish embryos. *PLoS ONE* **6**, e19713.
Jiménez-Amilburu, V., Rasouli, S. J., Staudt, D. W., Nakajima, H., Chiba, A., Mochizuki, N. and Stainier, D. Y. R. (2016). In vivo visualization of cardiomyocyte apicobasal polarity reveals epithelial to mesenchymal-like transition during cardiac trabeculation. *Cell Rep.* **17**, 2687-2699.
Johnson, R. and Halder, G. (2014). The two faces of Hippo: targeting the Hippo pathway for regenerative medicine and cancer treatment. *Nat. Rev. Drug Discov.* **13**, 63-79.
Kim, J. H., Lee, S.-R., Li, L.-H., Park, H.-J., Park, J.-H., Lee, K. Y., Kim, M.-K., Shin, B. A. and Choi, S.-Y. (2011). High cleavage efficiency of a 2A peptide derived from porcine teschovirus-1 in human cell lines, zebrafish and mice. *PLoS ONE* **6**, e18556.

Kim, J., Kim, Y. H., Kim, J., Park, D. Y., Bae, H., Lee, D.-H., Kim, K. H., Hong, S. P., Jang, S. P., Kubota, Y. et al. (2017). YAP/TAZ regulates sprouting angiogenesis and vascular barrier maturation. *J. Clin. Invest.* **127**, 3441-3461.

Kimelman, D., Smith, N. L., Lai, J. K. H. and Stainier, D. Y. R. (2017). Regulation of posterior body and epidermal morphogenesis in Zebrafish by localized Yap1 and Wwtr1. *Elife* **6**, e31065.

Komuro, A., Nagai, M., Navin, N. E. and Sudol, M. (2003). WW domain-containing protein YAP associates with ErbB-4 and acts as a co-transcriptional activator for the carboxyl-terminal fragment of ErbB-4 that translocates to the nucleus. *J. Biol. Chem.* **278**, 33334-33341.

Lee, K.-F., Simon, H., Chen, H., Bates, B., Hung, M. C. and Hauser, C. (1995). Requirement for neuregulin receptor erbB2 in neural and cardiac development. *Nature* **378**, 394-398.

Li, Y., Klena, N. T., Gabriel, G. C., Liu, X., Kim, A. J., Lemke, K., Chen, Y., Chatterjee, B., Devine, W., Damerla, R. R. et al. (2015). Global genetic analysis in mice unveils central role for cilia in congenital heart disease. *Nature* **521**, 520-524.

Liao, Y., Smyth, G. K. and Shi, W. (2014). featureCounts: an efficient general purpose program for assigning sequence reads to genomic features. *Bioinformatics* **30**, 923-930.

Lin, Y.-F., Swinburne, I. and Yelon, D. (2012). Multiple influences of blood flow on cardiomyocyte hypertrophy in the embryonic zebrafish heart. *Dev. Biol.* **362**, 242-253.

Linn, H., Ermekova, K. S., Rentschler, S., Sparks, A. B., Kay, B. K. and Sudol, M. (1997). Using molecular repertoires to identify high-affinity peptide ligands of the WW domain of human and mouse YAP. *Biol. Chem.* **378**, 531-537.

Liu, J., Bressan, M., Hassel, D., Huisken, J., Staudt, D., Kikuchi, K., Poss, K. D., Mikawa, T. and Stainier, D. Y. R. (2010). A dual role for ErbB2 signaling in cardiac trabeculation. *Development* **137**, 3867-3875.

Love, M. I., Huber, W. and Anders, S. (2014). Moderated estimation of fold change and dispersion for RNA-seq data with DESeq2. *Genome Biol.* **15**, 550.

Lu, L., Li, Y., Kim, S. M., Bossuyt, W., Liu, P., Qiu, Q., Wang, Y., Halder, G., Finegold, M. J., Lee, J.-S. et al. (2010). Hippo signaling is a potent in vivo growth and tumor suppressor pathway in the mammalian liver. *Proc. Natl. Acad. Sci. USA* **107**, 1437-1442.

Lyons, D. A., Pogoda, H.-M., Voas, M. G., Woods, I. G., Diamond, B., Nix, R., Arana, N., Jacobs, J. and Talbot, W. S. (2005). erbb3 and erbb2 are essential for schwann cell migration and myelination in zebrafish. *Curr. Biol.* **15**, 513-524.

Ma, X., Takeda, K., Singh, A., Yu, Z.-X., Zerfas, P., Blount, A., Liu, C., Towbin, J. A., Schneider, M. D., Adelstein, R. S. et al. (2009). Conditional ablation of nonmuscle myosin II-B delineates heart defects in adult mice. *Circ. Res.* **105**, 1102-1109.

Manderfield, L. J., Aghajanian, H., Engleka, K. A., Lim, L. Y., Liu, F., Jain, R., Li, L., Olson, E. N. and Epstein, J. A. (2015). Hippo signaling is required for Notch-dependent smooth muscle differentiation of neural crest. *Development* **142**, 2962-2971.

Meyer, D. and Birchmeier, C. (1995). Multiple essential functions of neuregulin in development. *Nature* **378**, 386-390.

Miesfeld, J. B., Gestri, G., Clark, B. S., Flinn, M. A., Poole, R. J., Bader, J. R., Besharse, J. C., Wilson, S. W. and Link, B. A. (2015). Yap and Taz regulate retinal pigment epithelial cell fate. *Development* **142**, 3021-3032.

Monier, B., Gettings, M., Gay, G., Mangeat, T., Schott, S., Guarner, A. and Suzanne, M. (2015). Apico-basal forces exerted by apoptotic cells drive epithelium folding. *Nature* **518**, 245-248.

Nakajima, H., Yamamoto, K., Agarwala, S., Terai, K., Fukui, H., Fukuhara, S., Ando, K., Miyazaki, T., Yokota, Y., Schmelzer, E. et al. (2017). Flow-dependent endothelial YAP regulation contributes to vessel maintenance. *Dev. Cell* **40**, 523-536.e6.

Ninov, N., Borius, M. and Stainier, D. Y. R. (2012). Different levels of Notch signaling regulate quiescence, renewal and differentiation in pancreatic endocrine progenitors. *Development* **139**, 1557-1567.

Ozcelik, C., Erdmann, B., Pilz, B., Wettschureck, N., Britsch, S., Hübner, N., Chien, K. R., Birchmeier, C. and Garratt, A. N. (2002). Conditional mutation of the ErbB2 (HER2) receptor in cardiomyocytes leads to dilated cardiomyopathy. *Proc. Natl. Acad. Sci. USA* **99**, 8880-8885.

Peshkovsky, C., Totong, R. and Yelon, D. (2011). Dependence of cardiac trabeculation on neuregulin signaling and blood flow in zebrafish. *Dev. Dyn.* **240**, 446-456.

Rasouli, S. J. and Stainier, D. Y. R. (2017). Regulation of cardiomyocyte behavior in zebrafish trabeculation by Neuregulin 2a signaling. *Nat. Commun.* **8**, 15281.

Reischauer, S., Arnaout, R., Ramadass, R. and Stainier, D. Y. R. (2014). Actin binding GFP allows 4D in vivo imaging of myofilament dynamics in the zebrafish heart and the identification of Erbb2 signaling as a remodeling factor of myofibril architecture. *Circ. Res.* **115**, 845-856.

Revenu, C., Streichan, S., Donà, E., Lecaudey, V., Hufnagel, L. and Gilmour, D. (2014). Quantitative cell polarity imaging defines leader-to-follower transitions during collective migration and the key role of microtubule-dependent adherens junction formation. *Development* **141**, 1282-1291.

Rottbauer, W., Saurin, A. J., Lickert, H., Shen, X., Burns, C. G., Wo, Z. G., Kemler, R., Kingston, R., Wu, C. and Fishman, M. (2002). Reptin and pontin antagonistically regulate heart growth in zebrafish embryos. *Cell* **111**, 661-672.

Samsa, L. A., Givens, C., Tzima, E., Stainier, D. Y. R., Qian, L. and Liu, J. (2015). Cardiac contraction activates endocardial Notch signaling to modulate chamber maturation in zebrafish. *Development* **142**, 4080-4091.

Saw, T. B., Doostmohammadi, A., Nier, V., Kocgozlu, L., Thampi, S., Toyama, Y., Marcq, P., Lim, C. T., Yeomans, J. M. and Ladoux, B. (2017). Topological defects in epithelia govern cell death and extrusion. *Nature* **544**, 212-216.

Schindelin, J., Arganda-Carreras, I., Frise, E., Kaynig, V., Longair, M., Pietzsch, T., Preibisch, S., Rueden, C., Saalfeld, S., Schmid, B. et al. (2012). Fiji: an open-source platform for biological-image analysis. *Nat. Methods* **9**, 676-682.

Sehnert, A. J., Huq, A., Weinstein, B. M., Walker, C., Fishman, M. and Stainier, D. Y. R. (2002). Cardiac troponin T is essential in sarcomere assembly and cardiac contractility. *Nat. Genet.* **31**, 106-110.

Staudt, D. and Stainier, D. (2012). Uncovering the molecular and cellular mechanisms of heart development using the zebrafish. *Annu. Rev. Genet.* **46**, 397-418.

Staudt, D. W., Liu, J., Thorn, K. S., Stuurman, N., Liebling, M. and Stainier, D. Y. R. (2014). High-resolution imaging of cardiomyocyte behavior reveals two distinct steps in ventricular trabeculation. *Development* **141**, 585-593.

Teng, X., Qin, L., Le, Borgne, R. and Toyama, Y. (2017). Remodeling of adhesion and modulation of mechanical tensile forces during apoptosis in Drosophila epithelium. *Development* **144**, 95-105.

Thisse, C. and Thisse, B. (2008). High-resolution in situ hybridization to whole-mount zebrafish embryos. *Nat. Protoc.* **3**, 59-69.

Totaro, A., Castellan, M., Battilana, G., Zanconato, F., Azzolin, L., Giulitti, S., Cordenonsi, M. and Piccolo, S. (2017). YAP/TAZ link cell mechanics to Notch signalling to control epidermal stem cell fate. *Nat. Commun.* **8**, 15206.

Toyama, Y., Peralta, X. G., Wells, A. R., Kiehart, D. P. and Edwards, G. S. (2008). Apoptotic force and tissue dynamics during Drosophila embryogenesis. *Science* **321**, 1683-1686.

Tullio, A. N., Accili, D., Ferrans, V. J., Yu, Z. X., Takeda, K., Grinberg, A., Westphal, H., Preston, Y. A. and Adelstein, R. S. (1997). Nonmuscle myosin II-B is required for normal development of the mouse heart. *Proc. Natl. Acad. Sci. USA* **94**, 12407-12412.

Vassilev, A., Kaneko, K. J., Shu, H., Zhao, Y. and DePamphilis, M. L. (2001). TEAD/TEF transcription factors utilize the activation domain of YAP65, a Src/Yes-associated protein localized in the cytoplasm. *Genes Dev.* **15**, 1229-1241.

von Gise, A., Lin, Z., Schlegelmilch, K., Honor, L. B., Pan, G. M., Buck, J. N., Ma, Q., Ishiwata, T., Zhou, B., Camargo, F. D. et al. (2012). YAP1, the nuclear target of Hippo signaling, stimulates heart growth through cardiomyocyte proliferation but not hypertrophy. *Proc. Natl. Acad. Sci. USA* **109**, 2394-2399.

Welikson, R. E. and Fischman, D. A. (2002). The C-terminal IgI domains of myosin-binding proteins C and H (MyBP-C and MyBP-H) are both necessary and sufficient for the intracellular crosslinking of sarcomeric myosin in transfected non-muscle cells. *J. Cell Sci.* **115**, 3517-3526.

Wickham, H. (2010). *ggplot2: Elegant Graphics for Data Analysis*. New York: Springer.

Wu, S., Huang, J., Dong, J. and Pan, D. (2003). hippo encodes a Ste-20 family protein kinase that restricts cell proliferation and promotes apoptosis in conjunction with salvador and warts. *Cell* **114**, 445-456.

Xin, M., Kim, Y., Sutherland, L. B., Qi, X., McAnally, J., Schwartz, R. J., Richardson, J. A., Bassel-Duby, R. and Olson, E. N. (2011). Regulation of insulin-like growth factor signaling by Yap governs cardiomyocyte proliferation and embryonic heart size. *Sci. Signal.* **4**, ra70.

Xin, M., Olson, E. N. and Bassel-Duby, R. (2013a). Mending broken hearts: cardiac development as a basis for adult heart regeneration and repair. *Nat. Rev. Mol. Cell Biol.* **14**, 529-541.

Xin, M., Kim, Y., Sutherland, L. B., Murakami, M., Qi, X., McAnally, J., Porrello, E. R., Mahmoud, A. I., Tan, W., Shelton, J. M. et al. (2013b). Hippo pathway effector Yap promotes cardiac regeneration. *Proc. Natl. Acad. Sci. USA* **110**, 13839-13844.

Yu, F.-X., Zhao, B. and Guan, K.-L. (2015). Hippo pathway in organ size control, tissue homeostasis, and cancer. *Cell* **163**, 811-828.

Zhao, B., Ye, X., Yu, J., Li, L., Li, W., Li, S., Yu, J., Lin, J. D., Wang, C.-Y., Chinnaiyan, A. M. et al. (2008). TEAD mediates YAP-dependent gene induction and growth control. *Genes Dev.* **22**, 1962-1971.

Zhao, B., Li, L., Tumaneng, K., Wang, C.-Y. and Guan, K.-L. (2010). A coordinated phosphorylation by Lats and CK1 regulates YAP stability through SCF(beta-TRCP). *Genes Dev.* **24**, 72-85.